Electron-phonon interactions in the high-temperature superconductors

Ju H. Kim,* K. Levin, and R. Wentzcovitch†
The University of Chicago, Department of Physics and The James Franck Institute, Chicago, Illinois 60637

A. Auerbach
Physics Department, Boston University, Boston, Massachusetts 02215

(Received 30 July 1990; revised manuscript received 20 February 1991)

A characterization of the electron-phonon coupling in the high-temperature superconductors is important both in helping to ascertain the role of phonons in the superconductivity and in helping to characterize the phonon "background" contribution to the temperature-dependent resistivity. Here we present a "frozen phonon" and equivalent diagrammatic scheme for calculating the electron-phonon coupling in the presence of very strong Coulomb correlations. The inclusion of these correlations is essential for creating the insulating state at half-filling. Furthermore, these effects substantially reduce the electron-phonon contribution to the resistivity, so that the experimentally measured coupling constant of the resistivity $\lambda \simeq 0.2$–0.4 can be reconciled with the necessarily smaller electron-phonon contribution. Our frozen-phonon scheme is based on a Coulomb renormalized band structure of the copper-oxygen plane alone. Coulomb correlations lead to a suppression of charge fluctuations as the insulator is approached and thereby a significant reduction in the electron-phonon coupling. Low-frequency modes ($\omega \simeq 12$ meV) imply a quasilinear phonon resistivitiy down to temperatures of the order of 50 K. This band structure also provides reasonable values for the plasma frequency, which like the experimental measurements show a decrease as the insulator is approached. This can be attributed physically to an enhanced effective mass, which is a precursor to Mott localization at half-filling. The combination of the plasma frequency and electron-phonon coupling leads to a relatively concentration-independent resistivity slope, whose magnitude accounts for a large fraction of the measured linear resistivity at moderate and high hole concentrations x. However, this phonon background is significantly less than the measured resistivity slope as the insulator is approached. This suggests that electron-electron scattering may be playing a more dominant role at small x. Following the Mott-Ioffe-Regel criterion, we analyze the implications of our results for the breakdown of the metallic state at finite concentrations x. We conclude with the observation that the strength of the electron-phonon interaction appears to us from transport data, as well as our microscopic calculations to be too weak to be the primary mechanism responsible for high-temperature superconductivity. On the other hand, we cannot with certainty rule this mechanism out.

I. INTRODUCTION

Because of the evidently renewed interest in phonon mechanisms for explaining high-temperature superconductivity, it is important to study microscopically the electron-phonon coupling in some detail. In such studies it is, furthermore, essential to keep two factors in mind: (1) the metallic cuprates have evolved from Mott insulators, so that strong Coulomb correlations are present in these systems and (2) transport data have now been sufficiently analyzed so that the constraints imposed by such data on the electron-phonon interaction must be taken into account. In this paper we study the nature of the electron-phonon interactions in doped Mott insulators such as the two-dimensional metallic cuprates, paying particular attention to these two factors. We find that strong Coulomb correlation effects lead to a significant screening of the electron-phonon coupling in the metallic phase. This screening becomes progressively more important as the insulator is approached. We then determine the role of this coupling on the temperature and hole concentration dependence of the electrical resistivity.

Since the discovery of high-temperature superconductivity in the copper oxides, many theories have been proposed[1] to provide a consistent explanation for both normal and superconducting properties. There is, however, no clear agreement on the appropriate theoretical description for these materials even in their normal state, and it is generally believed that characterizing the cuprates above T_c is a necessary first step in unraveling the superconducting mechanism. In view of recent photoemission data,[2] which shows some features of the calculated local-density-approximation (LDA) band structure, Fermi-liquid-based approaches must be taken seriously. In a series of papers, we have undertaken a systematic analysis of the normal-state magnetic[3] and transport[4] properties using a Fermi-liquid-based scheme. The present paper is a continuation of this study and represents a longer version of a previous short publication on the electron-phonon coupling.[4] In our picture, the ground state, in the absence of superconductivity, is as-

sumed to correspond to a Fermi liquid. However, on the basis of both phenomenological[5] and microscopic[3,4] analyses, we have found that the characteristic degeneracy temperature of the Fermi liquid is relatively low. Near optimal stoichiometry the metallic cuprates behave as fully coherent Fermi liquids only at temperatures below 100–350 K. Above this "coherence" temperature, $T_{\rm coh}$, the d electrons begin to show signs of incipient localization.

Our picture is highly influenced by similar behavior in the heavy-fermion metals (which are generally described by an analogous Hamiltonian) and where the f electrons are the direct counterpart of the Cu $3d$ states and the characteristic energy scale $T_{\rm coh}$ is roughly 2 orders of magnitude smaller. The anomalies exhibited in the heavy fermions above 1–2 K are similar to those seen in the cuprates above 100–200 K. Thus, the NMR relaxation shows deviations from Korringa behavior, the Hall coefficient R_H assumes a large magnitude and is temperature dependent. Finally, the resistivity is found to exhibit deviations from the canonical T^2 dependence of a Fermi liquid. All of these phenomena have their counterparts in the copper oxides,[5,6] albeit at higher temperatures, and all of these have been interpreted in the heavy fermions as arising from the loss of full f-electron coherence. Ultimately, in the heavy-fermion metals, the f electrons behave as independent local moments, although this occurs at high temperatures ($T \approx 150$ K) so that the counterpart phenomenon in the cuprates would not be experimentally accessible. A summary of our picture of the cuprates would characterize them as "partially coherent" Fermi liquids over much, if not all, of the normal-state temperature regime and this may explain the many anomalies seen in the normal state. This Fermi-liquid scheme is in the general category of "almost localized" Fermi liquids to which also belong the quantum liquid, ^{3}He, and the heavy-fermion metals.

As further support for this picture, it should be noted that, in those cuprates which have hole concentrations in excess of the "optimal" concentration for superconductivity, many Fermi-liquid-like features are observed. In these overdoped, but still superconducting, samples, R_H is found to approach a smaller and temperature-independent value, the NMR relaxation appears more Korringa-like[7] and a T^2 contribution to the resistivity has been observed.[8] This is consistent with the physical picture we have proposed[9] in which the coherence energy scale $T_{\rm coh}$ monotonically increases with hole concentration. The half-filled insulator, which corresponds to a Mott localized state, is associated with $T_{\rm coh}=0$. Coherent Fermi-liquid behavior is observable in the normal state when $T_c/T_{\rm coh}<1$, which thus corresponds in our theory to "overdoped" systems. In contrast, as the insulator is approached, $T_{\rm coh}$ becomes sufficiently small so that the entire normal-state temperature region is outside of the Fermi-liquid regime.

Indeed, our microscopic calculations support this more phenomenologically derived picture. Using a (coherent) Fermi-liquid picture, we find good agreement[9] with Hall coefficient data until x decreases to about $x=0.10$–0.15 in $La_{2-x}Sr_xCuO_4$ systems. The electron-phonon contribution to the resistivity, which will be presented below, is also found to account[4] for most of the measured value of the resistivity slope until hole concentrations $x \simeq 0.10$–0.15, where it becomes clear that some inelastic-scattering mechanism, other than the traditional electron-phonon coupling, must be dominating the resistivity. We speculate that the breakdown of a Fermi-liquid-based explanation of the Hall data is due to an "extraordinary" Hall effect, such as is present in heavy fermions.[10] Similarly, the additional inelastic scattering seen in the resistivity data may arise from electron-electron scattering which evidently becomes stronger as the insulator is approached.

Within this physical picture our calculation of the electron-phonon interaction provides an estimate of the associated "background" contribution to the resistivity. We demonstrate that, because of low-lying phonon modes, the electron-phonon component of the resistivity is nearly linear above T_c. We stress that our calculations do not imply that the remarkably linear resistivity of the cuprates is entirely due to phonons, but rather that they contribute a significant fraction of the resistivity slope. As a result their contribution must be subtracted in order to ascertain the importance of other more exotic scattering contributions to the resistivity. We believe that ignoring this phonon contribution in attempting to fit the linear resistivity, as is generally done,[11] is incorrect. On the other hand, it is equally incorrect to take the point of view that phonons are the sole source of this linearity.

To assess the general transport properties and the importance of phonons in the copper oxides, we list some of the conclusions drawn from experiments which need to be explained.

(1) The linear resistivity persists through a wide range of temperature without any indication of saturation.[12] This has been interpreted as indicating that the mean free path of an electron is larger than the copper-oxygen bond length and the overall inelastic coupling constant λ is small.[12]

(2) The plasma frequency ω_p of the copper oxides, which is found to be T independent, ranges[13,14] from 0.8 to 1.6 eV which is about roughly $\frac{1}{10}$ of the corresponding value in transition metals such as Cu and Ag.[15] The concentration dependence is found to be $\omega_p \propto \sqrt{x}$ for both $La_{2-x}Sr_xCuO_4$ and $YBa_2Cu_3O_{7-\delta}$ (where δ can be related to x using simple stoichiometry arguments) as is shown in Fig. 1(a). Because $\omega_P^2 \propto n/m^*$, this may be interpreted as either a decreasing carrier number $n \propto x$ or as an increasing effective mass $m^* \propto 1/x$ as the insulator is approached.

(3) The scattering lifetime τ in the copper oxides[16,13,14] is approximately 5×10^{-14} sec and it is almost concentration independent as shown in Fig. 1(b). This measured value of τ is roughly $\frac{1}{10}$ of the value in metallic copper. The appropriate inelastic coupling constant λ defined by $\tau^{-1}=2\pi\lambda T$ is roughly 0.2–0.4, which provides an upper bound for the electron-phonon coupling.

(4) The slope of the resistivity increases dramatically as the metal-insulator transition is approached.[4,17] The overall variation in slope is almost a factor of 100, but throughout most of the metallic regime the concentration

dependence is rather weak. These trends which are fairly universal in the cuprates have not been given much prior attention, although it is our opinion that they provide an important constraint on the nature of the linear resistivity.

In contrast to previous calculations,[18] the present work emphasizes the importance of Coulomb correlations for calculations of the electron-phonon interaction. Previous LDA-based or weakly Coulomb correlated theories of this interaction have led to some inconsistencies. All Fermi-liquid approaches must explain at the same time a small coupling constant and a moderately heavy effective mass which is seen in ac conductivity Drude fits. These two properties would seem to be incompatible in conventional theories where the source of the effective mass is the electron-phonon self energy. Although Allen and co-workers have shown that a quasilinear resistivity is obtained from the phonon contribution,[18] Gurvitch and Fiory have argued that their LDA results do not satisfy[12] the Mott-Ioffe-Regel condition[19] in which the mean free path of electrons must be larger than the minimum scattering length. The data are, however, consistent with the present picture in which, although the phonons are weakly coupled to electrons, strong Coulomb correlations are responsible for the large effective mass or low plasma frequency.[20]

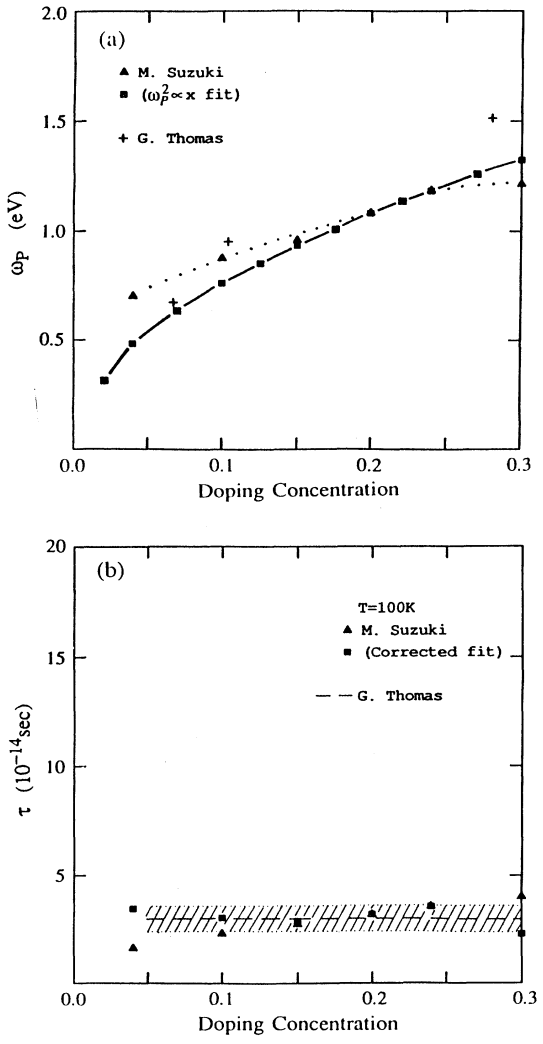

FIG. 1. Experimentally measured (a) plasma frequency and (b) transport lifetime as a function of doping concentration. The triangles indicate strontium doping in La_2CuO_4 from Ref. 13 and the squares represent a $\omega_P^2 \propto x$ fit of this data (for x around optimal doping). The crosses in (a) indicate oxygen concentration dependence in $YBa_2Cu_3O_{7-\delta}$ from Ref. 16 scaled to an effective hole concentration x. "Corrected fit" in (b) corresponds to fitted data (squares) in (a).

We outline the remainder of this paper. In Sec. II A we discuss our frozen-phonon approach for calculating the electron-phonon transition matrix element for a two-dimensional zone edge ($\mathbf{q}=\mathbf{X}$) phonon in the presence of strong Coulomb correlations. In Sec. II B these results are reproduced using a diagrammatic (auxiliary boson) formalism. Here the wave vector is taken to be arbitrary. Finally, in Sec. III we discuss various transport properties which result from these electron-phonon interactions and present comparisons with a variety of experiments. The reader who is uninterested in the formal aspects may skip directly to Sec. III. Many of the complicated details of our calculations are relegated to Appendices A and B.

II. FORMAL RESULTS

In this section, we calculate the electron-phonon interaction using the frozen-phonon method. This technique is often applied[21] to deduce electron-phonon coupling in the context of more conventional band-structure approaches which are highly numerical. Here we proceed somewhat more analytically. Our starting point is the three-band Hubbard Hamiltonian which describes the copper-oxide plane. Following the work[22] of McMahan, Martin, and Satpathy, we construct a semirealistic model Hamiltonian which includes a next-nearest-neighbor interaction (i.e., oxygen-oxygen overlap)

$$
\begin{aligned}
H = & \sum_{j,\eta,\sigma} \varepsilon_p C_{j,\sigma}^{\eta\dagger} C_{j,\sigma}^{\eta} + \sum_{i,\sigma} \varepsilon_d^0 D_{i,\sigma}^{\dagger} D_{i,\sigma} \\
& + \sum_{\langle ij \rangle,\eta,\sigma} V_{i,j} (C_{j,\sigma}^{\eta\dagger} D_{i,\sigma} + D_{i,\sigma}^{\dagger} C_{j,\sigma}^{\eta}) \\
& + \sum_{\langle jl \rangle(\eta \neq \eta'),\sigma} t_{j,l} (C_{j,\sigma}^{\eta\dagger} C_{l,\sigma}^{\eta'} + C_{l,\sigma}^{\eta'\dagger} C_{j,\sigma}^{\dagger}) \\
& + \sum_i U_d n_{i,\uparrow} n_{i,\downarrow} , \qquad (2.1)
\end{aligned}
$$

where ε_p and ε_d^0 are the oxygen and (unrenormalized) copper energy levels, $C_{j,\sigma}^{\eta\dagger}$ ($C_{j,\sigma}^{\eta}$) and $D_{i,\sigma}^{\dagger}$ ($D_{i,\sigma}$) are creation (destruction) operators for the oxygen electrons at site j and spin σ and copper electrons at site i, with spin σ, respectively. The hopping interaction $V_{i,j}$ is between neighboring copper and oxygen sites, while $t_{j,l}$ describes the transfer between two nearest-neighbor oxygen sites, and $n_{i,\sigma} = D_{i,\sigma}^{\dagger} D_{i,\sigma}$. Here η ($=x,y$) represents two oxygen orbitals (p_x and p_y), and $\langle jl \rangle$ ($\eta \neq \eta'$) denotes the nearest-neighboring orbitals η and η' at sites j and l, re-

spectively. The Coulomb repulsion between electrons on Cu sites is U_d.

It is generally assumed that U_d is the largest energy scale in the problem. At infinite U_d, a mean-field theory may be derived using the auxiliary boson approach; this model has been extensively studied by ourselves[3–5,9] and, in slightly different variations, by others.[23] It is based on a $1/N$ expansion, where N is the spin degeneracy of the Cu and O sites. Here we work in the electron picture (although similar results also can be derived in the "hole" picture). This allows us to take semirealistic values for the parameters in Eq. (2.1) and still preserve the Mott localization ($m^* \rightarrow \infty$) at half-filling. This localization arises from a suppression of the renormalized hybridization as $x \rightarrow 0$.

In the limit of infinite U_d, we introduce an auxiliary boson $\mathbf{e}_i$ which corresponds to the Cu^{3+} valence state, in which the $d_{x^2-y^2}$ state is empty. The fermion operator $d_{i,\sigma}$ represents a Cu^{2+} state with spin σ. In this case, the $d_{x^2-y^2}$ level is $\frac{1}{2}$ full. Imposing the constraint via a Lagrange multiplier λ_i at each site that there be no double occupancy of the $d_{x^2-y^2}$ orbital requires that

$$\sum_\sigma d_{i,\sigma}^\dagger d_{i,\sigma} + \mathbf{e}_i^\dagger \mathbf{e}_i = 1 \ . \tag{2.2}$$

In the mean-field limit, the operator $\mathbf{e}_i$ is replaced by its expectation value $\mathbf{e}_0$ which is spatially uniform and similarly λ_i is replaced by the average λ_0 so that the Hamiltonian may be written as

$$\begin{aligned} H_{\rm mf} = & \sum_{j,\eta,\sigma} \varepsilon_p C_{j,\sigma}^{\eta\dagger} C_{j,\sigma}^{\eta} + \sum_{i,\sigma} \varepsilon_d d_{i,\sigma}^\dagger d_{i,\sigma} \\ & + \sum_{\langle ij \rangle,\eta,\sigma} V e_0 (C_{j,\sigma}^{\eta\dagger} d_{i,\sigma} + \text{H.c.}) \\ & + \sum_{\langle jl \rangle,\eta\neq\eta',\sigma} t (C_{j,\sigma}^{\eta\dagger} C_{l,\sigma}^{\eta'} + \text{H.c.}) \ . \end{aligned} \tag{2.3}$$

Finally the parameters e_0 and λ_0 may be variationally obtained by minimizing the resulting mean-field free energy. A diagonalization of the Hamiltonian [Eq. (2.3)] for the case of zero oxygen-oxygen overlap $t=0$ yields a simple dispersion relation $E_{\mathbf{k}}^{\pm}$ for the renormalized band structure

$$\begin{aligned} E_{\mathbf{k}}^{\pm} &= \frac{\varepsilon_p + \varepsilon_d}{2} \pm \left[\left(\frac{\varepsilon_p - \varepsilon_d}{2} \right)^2 + r_0^2 \gamma_{\mathbf{k}}^2 \right]^{1/2} \\ &= \varepsilon_d \pm r_0 \gamma_{\mathbf{k}} (\cot\theta_k)^{\pm 1} \ . \end{aligned} \tag{2.4a}$$

In Eq. (2.4a), $\varepsilon_d = \varepsilon_d^0 + \lambda_0$, $r_0 = e_0 V$, and the dispersion

$$\gamma_{\mathbf{k}}^2 = 4 \left[\cos^2 \frac{k_x a}{2} + \cos^2 \frac{k_y a}{2} \right] \tag{2.4b}$$

arises entirely from the hopping terms between copper and oxygen orbitals. Associated with the eigenenergies of the mean-field Hamiltonian are the eigenstates $\alpha_{\mathbf{k},\sigma}$, $\beta_{\mathbf{k},\sigma}$, and $\delta_{\mathbf{k},\sigma}$ which correspond to the antibonding, bonding, and nonbonding states, respectively. In most of this paper we consider the case of nonzero t, so that $E_{\mathbf{k}}$ does not reduce to a simple expression.

It may be seen that the effects of infinite U_d are twofold: (1) the renormalized hybridization $r_0 = e_0 V$ is greatly reduced, particularly as the half-filled limit is approached, since double occupancy of the d site must be avoided, and (2) the position of the d level ε_d is renormalized in order to accommodate no more than one electron in the d orbital. The former effect thus corresponds to Mott localization of the d electrons, which, in the metallic phase, is responsible for the low-energy scale $T_{\rm coh}$ discussed above. This, in turn, arises from the factor e_0 which vanishes as the hole concentration approaches zero.

A. Frozen-phonon study

The procedure for calculating the electron-phonon coupling within the frozen-phonon scheme involves a standard sequence of steps applied to this renormalized band structure. First the frozen phonon (with characteristic wave vector $\mathbf{q}$) is introduced as a static displacement of the ions within the 2D copper-oxide plane. Next, the electronic dispersion is recomputed in the presence of this distortion. Comparison with the electronic energy in the undistorted lattice indicates a "mixing" of states having wave vector $\mathbf{k}$ with those of $\mathbf{k}+\mathbf{q}$. The associated transition matrix element is readily related to the electron-phonon coupling at wave vector $\mathbf{q}$.

In the present paper we extend the standard frozen-phonon calculations to include the strong Coulomb correlations which are believed to lead to the insulating state of the cuprates at half filling. These Coulomb correlations are incorporated via the renormalized band structure which is derived from Eq. (2.3) and its extension, in the presence of a frozen phonon. To provide an overview of the general formulation, a simpler example, which focuses on a 1D model containing both Cu and O components, is presented in Appendix A. In order to clarify the present application of the frozen-phonon scheme, we first summarize the relevant notation and vocabulary.

The electron-phonon Hamiltonian is written in terms of a vector representation of the quasiparticle basis operators $\Phi_{k,\sigma}$. These basis operators, deduced from a diagonalization of the (undistorted) Hamiltonian [Eq. (2.3)], are the eigenstates $\alpha_{\mathbf{k},\sigma}$, $\alpha_{\mathbf{k}+\mathbf{q},\sigma}$, etc., which were referred to earlier. The difference between the distorted and undistorted Hamiltonians is called $\mathbf{M}_D$, which is directly related to the electron-phonon coupling. A natural basis for representing this difference matrix is the band representation, $C_{k,\sigma}^{\eta}$, and $d_{k,\sigma}$, corresponding to the various oxygen and copper electron operators. Thus, $\mathbf{M}_D$ contains contributions from changes (induced by the static distortion) in the copper-oxygen hybridization, the d-band center of gravity, and the oxygen-oxygen overlap. The values of these shifts are linear in the ionic displacement and their "bare" values can be deduced following Ref. 24. Conversion of $\mathbf{M}_D$ to the quasiparticle basis $\alpha_{\mathbf{k},\sigma}$ involves a unitary transformation U.

In the strong-U_d limit, the matrix $\mathbf{M}_D$ is self-consistently derived. In this way, important screening effects enter as renormalizations of the *bare shifts* in the copper-oxygen hybridization and d-band center of gravity. These self-consistently obtained[25] screening contribu-

tions are parametrized in terms of the quantities e_0 and λ_0.

In order to make analytical progress, we further simplify the ionic component by considering only the zone edge ($\mathbf{q}=\mathbf{X}=\pi/a$) phonons. These **X** phonons appear to couple most effectively since they lead to strong perturbations in the crystalline potential associated with charge transfer between like atoms. In contrast to these longitudinal modes, correlation effects deriving from the transverse modes at $\mathbf{q}=\mathbf{X}$ are not as dramatic since they maintain the equivalence of like atoms. Because there are a large number of **X** phonons in two dimensions, we build on the lattice-dynamics calculation of Ref. 26. In La_2CuO_4 in the tetragonal phase, a potential induced breathing model shows that there are 21 modes, 4 of which are unstable.[27] It is not at all clear how to incorporate these unstable modes in a consistent fashion. Furthermore, the associated motion appears to couple only weakly to the electronic degrees of freedom. Hence, we ignore these negative-frequency modes here. The remaining 17 modes are categorized by considering only the motion of those copper and oxygen ions which are in the plane. Our simple 2D models do not distinguish between modes which involve motion of atoms, other than those in the plane. In this way, six distinct types of 2D copper-oxygen phonon modes are found. These are shown in Fig. 2.

Following this frozen-phonon (FP) procedure, we calculate the renormalized band structure and the quasiparticle states in the distorted (**X**-mode) lattice. The distorted Hamiltonian in the infinite U_d limit is written in terms of auxiliary boson operators[25] as

$$H_{\mathrm{FP}}^{2d}=\sum_{i,n,\sigma}\varepsilon_{d,n}^{0}d_{\mathrm{i},n,\sigma}^{\dagger}d_{\mathrm{i},n,\sigma}+\sum_{\mathrm{i},m,\eta}\varepsilon_{p,m}^{\eta}C_{\mathrm{i},m,\sigma}^{\eta\dagger}C_{\mathrm{i},m,\sigma}^{\eta}+\sum_{\mathrm{i},n,\sigma}V_n(d_{\mathrm{i},n,\sigma}^{\dagger}\mathbf{e}_{\mathrm{i},n}\sum_{\delta,m,\eta}C_{\mathrm{i}+\delta,m,\sigma}^{\eta}+\mathrm{H.c.})+\tfrac{1}{2}\sum_{\mathrm{i},m,m',\sigma}\left[C_{\mathrm{i},m,\sigma}^{\eta\dagger}\sum_{\delta(\eta'\neq\eta)}t_{\delta}C_{\mathrm{i}+\delta,m',\sigma}^{\eta'}+\mathrm{H.c.}\right], \tag{2.5}$$

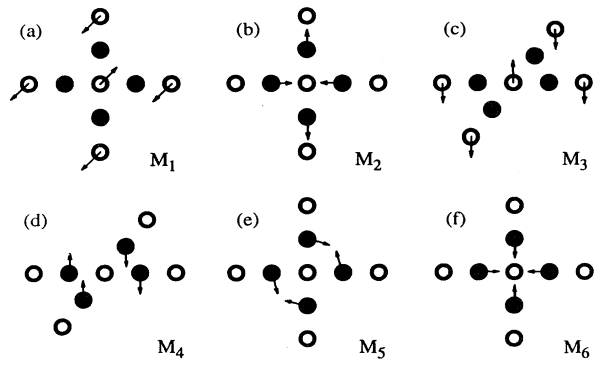

FIG. 2. The six planar modes projected from the lattice-dynamics calculation of Ref. 26. The open and solid circles indicate copper and oxygen, respectively.

where the index $n=1,2$ denotes two positions for the copper orbitals and the indices m ($=1,2$) denote two inequivalent oxygen sites. As in the undistorted case, the operators $\mathbf{e}_{in}^{\dagger}$ and $d_{\mathbf{in}}^{\dagger}$ create Cu^{3+} and Cu^{2+} states, respectively, whereas $C_{\mathrm{i},m,\sigma}^{\eta\dagger}$ creates an electron at the mth oxygen site within the ith unit cell. The constraint equations are imposed on each copper site

$$\sum_{\sigma}d_{\mathrm{i},n,\sigma}d_{\mathrm{i},n,\sigma}+\mathbf{e}_{\mathrm{i},n}\mathbf{e}_{\mathrm{i},n}=1\ . \tag{2.6}$$

Note $\langle\mathbf{e}_{\mathrm{i}1}\rangle$ is not identical to $\langle\mathbf{e}_{\mathrm{i}2}\rangle$ since the distortion changes the local environment of the two copper sites. A renormalized band structure is directly obtained from Eq. (2.5) by replacing the boson operators by their corresponding expectation values and introducing the constraint equation [Eq. (2.6)] via a Lagrange multiplier. Except for the states near $\mathbf{k}_{ZE}=\pm(\pi/2a)(1,1,0)$, the renormalized band structure obtained from a solution of the mean-field equations for H_{FP}^{2d} is similar to that obtained by folding the Brillouin zone (BZ) of the undistorted lattice. Following the details described in Appendix A for the simple 1D case, we express the quasiparticle operators as

$$\Phi_{\mathbf{k},\sigma}=\begin{bmatrix}\alpha_{\mathbf{k},\sigma}\\ \alpha_{\mathbf{k}+\mathbf{Q},\sigma}\\ \delta_{\mathbf{k},\sigma}\\ \delta_{\mathbf{k}+\mathbf{Q},\sigma}\\ \beta_{\mathbf{k},\sigma}\\ \beta_{\mathbf{k}+\mathbf{Q},\sigma}\end{bmatrix}=\mathbf{U}\cdot\begin{bmatrix}d_{1,\mathbf{k},\sigma}\\ d_{2,\mathbf{k},\sigma}\\ C_{1,\mathbf{k},\sigma}^{x}\\ C_{2,\mathbf{k},\sigma}^{x}\\ C_{1,\mathbf{k},\sigma}^{y}\\ C_{2,\mathbf{k},\sigma}^{y}\end{bmatrix}, \tag{2.7}$$

where the operators α, δ, and β destroy a quasiparticle in the antibonding, nonbonding, and bonding bands, respectively.

Within this mean-field approximation, the difference between the Hamiltonians corresponding to the distorted, H_{FP}^{2d}, and undistorted, H_0, cases may be readily deduced from Eqs. (2.5) and (2.3):

$$H_{e\text{-ph}}=H_{\mathrm{FP}}-H_0=\sum_{\mathbf{k},\sigma}\Phi_{\mathbf{k},\sigma}^{\dagger}\overline{\mathbf{M}}_D\Phi_{\mathbf{k},\sigma}+\sum_{n}\lambda_n(e_n^2-1)-2\lambda_0(e_0^2-1)\ , \tag{2.8}$$

where the λ_n's are Lagrange multipliers introduced to satisfy the constraint equation of (2.6) and $\overline{\mathbf{M}}_D=\mathbf{U}\cdot\mathbf{M}_D\cdot\mathbf{U}^{\dagger}$ is the transformed distortion matrix (which includes "screening" effects via the parameters e_n and λ_n).

In this analysis we focus on intraband scatterings between $\alpha_{\mathbf{k},\sigma}$ and $\alpha_{\mathbf{k}+\mathbf{X},\sigma}$ because these states near E_F are strongly scattered by the ionic displacement (zone-folding effect). Furthermore, other contributions such as interband scattering require higher energies than a phonon can provide. These intraband terms are written as

$$H_{e\text{-ph}}=\sum_{\mathbf{k},\sigma}\hat{\mathbf{g}}_{\mathbf{X}}(\alpha_{\mathbf{k},\sigma}^{\dagger}\alpha_{\mathbf{k}+\mathbf{X},\sigma}+\alpha_{\mathbf{k}+\mathbf{X},\sigma}^{\dagger}\alpha_{\mathbf{k},\sigma}). \tag{2.9a}$$

Here the electron-phonon coupling in the quasiparticle basis is

$$\hat{g}_{\mathbf{X}} = \langle \alpha_{\mathbf{k},\sigma} | H_{e\text{-ph}} | \alpha_{\mathbf{k}+\mathbf{X},\sigma} \rangle \ . \tag{2.9b}$$

We may express this matrix element in terms of phonon creation (destruction) operators $a^{\dagger}_{\mathbf{X},\nu}$ ($a_{\mathbf{X},\nu}$) for a wave vector $\mathbf{X}$ with quantized displacement (with $h=1$)

$$\hat{g}_{\mathbf{X},\nu} = g_{\mathbf{X},\nu} \left[\frac{1}{2N_0 M_{\mathbf{X},\nu} \omega_{\mathbf{X},\nu}} \right]^{1/2} (a^{\dagger}_{\mathbf{X},\nu} + a_{-\mathbf{X},\nu}) \ , \tag{2.10a}$$

where the electron-phonon transition matrix element is

$$g_{\mathbf{X},\nu} = \lim_{\delta \mathbf{R} \to 0} \left\langle \alpha_{\mathbf{k},\sigma} \left| \frac{\delta H}{\delta \mathbf{R}} \cdot \hat{\epsilon}_{\mathbf{X},\nu} \right| \alpha_{\mathbf{k}+\mathbf{X},\sigma} \right\rangle \tag{2.10b}$$

and $\hat{\epsilon}_{\mathbf{X},\nu}$ is the polarization vector for a normal mode ν. N_0 is the number of ions in each unit cell. $M_{\mathbf{X},\nu}$ is the reduced mass corresponding to a phonon mode $(\mathbf{X},\nu)$. Here, $\omega_{\mathbf{X},\nu}$ is a normal mode frequency.

The electron-phonon matrix elements in Eq. (2.10b) can now be evaluated in terms of changes in the "bare" Hamiltonian parameters which arise from a lattice distortion. Following Ref. 24, it may be seen that the overlap integral or hybridization between copper $3d_{x^2-y^2}$ and oxygen $2p$ orbital distance is highly anisotropic. A small distortion along the longitudinal direction (bonding axis) leads to significant changes in hybridization. This can be represented as linearly proportional to the ionic displacement when the distortion is small (see Appendix B)

$$V_n(\mathbf{R}+\delta\mathbf{R}) - V(\mathbf{R}) \approx \frac{\delta V}{\delta R} \delta R = -7V \frac{\delta \mathbf{R}}{a} \tag{2.11a}$$

and

$$t(\mathbf{R}+\delta\mathbf{R}) - t(\mathbf{R}) \approx -2t(\mathbf{R}) \frac{\delta \mathbf{R}}{a} \ . \tag{2.11b}$$

Along the transverse direction (perpendicular to the bonding axis), however, the change in hybridization is almost negligible. These changes in V ultimately lead to changes in the variational parameters such as e_n and λ_n. When these parameters are self-consistently calculated, they are found to vary linearly with displacement about the equilibrium (or undistorted) values e_0 and λ_0:

$$e_n \approx e_0 \pm \frac{\delta e_0}{\delta R} \delta R$$

and

$$\lambda_1 - \lambda_2 \approx \frac{\delta \lambda_0}{\delta R} \delta R \ , \tag{2.12}$$

where $\delta e_0/\delta R$ and $\delta\lambda_0/\delta R$ may be identified as the Coulomb correlation-induced screening responses. These functions depend on E_F and their concentration dependence may be calculated using a somewhat simplified analysis.[28]

Within this frozen-phonon scheme, the coupling constants are then numerically obtained. In Fig. 3, we plot the Fermi surface average $\langle\langle \ \rangle\rangle_{\mathrm{FS}}$ of the resulting electron-phonon matrix elements for the six types of $\mathbf{X}$ phonons shown in Fig. 2 as a function of concentration.[29] It is clear from Fig. 3 that the charge-transfer modes M_1, M_5, and M_6 couple to the electrons more strongly than others although their coupling is still weak compared to the zero Coulomb correlation case. The matrix elements for the copper charge-transfer modes (M_5 and M_6) are roughly three to four times larger than those of the oxygen charge-transfer mode (M_1). This is a result of the enhancement of the variational response by on-site Coulomb correlations. It is shown analytically, in Appendix B, that the various $\langle\langle g_{\mathbf{X},M_i} \rangle\rangle_{\mathrm{FS}}$ all vanish quadratically (in the bose amplitude) near the metal-insulator transition. However, near this transition the frozen-phonon picture will breakdown since the electronic energy scales then become comparable to those of the phonons. A more detailed discussion of this point is presented in Sec. III.

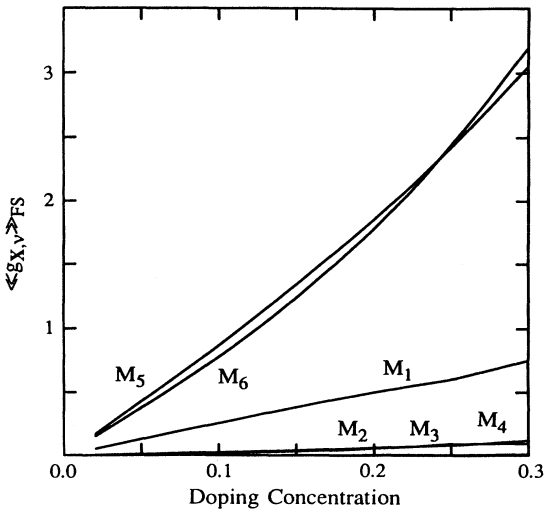

FIG. 3. Concentration dependence of the Fermi surface averaged electron-phonon transition matrix elements for the six planar modes shown in Fig. 2.

B. Diagrammatic calculation

In this section, the main results of the frozen-phonon calculation in Sec. II A are reproduced by using a diagrammatic auxiliary boson formalism. A similar, but independently derived, approach has been presented in Ref. 30 for the heavy-fermion problem. By evaluating the relevant Feynman diagrams, we show that the screened electron-phonon coupling constant, like the transition matrix elements, vanishes quadratically (in the Bose amplitude) near the metal-insulator transition. Although, in the diagrammatic formulation, the coupling constant can be calculated for an arbitrary wave vector with significantly less effort than with the frozen-phonon method, the details pertaining to the mode dependence of the coupling constants are often too difficult to extract. For this reason we calculate (to lowest order) the diagrams which represent the screened coupling constant. In Fig. 4, we show all diagrams within the mean-field order. Although the second diagram [Fig. 4(b)] may appear

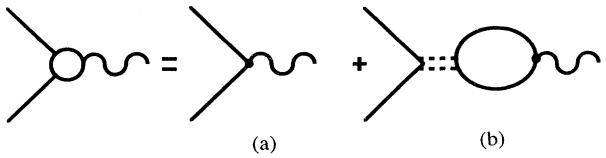

FIG. 4. Diagrams for the screened electron-phonon coupling constant. (a) and (b) refer to contributions from the renormalized band structure and the slave boson screening effect, respectively.

as order $O(1/N)$ because of the boson propagator, this, in fact, is a mean-field diagram (the summation over spin degeneracy in the polarization bubble cancels the $/1N$ factor). Since the goal here is to understand the screening effects from these diagrams as half-filling is approached, the second diagram must be included if we are to correctly account for the distortion-induced response.

For the purpose of simplicity, we exclude the oxygen-oxygen hopping terms and consider, as we have done in the frozen-phonon calculation, only intraband scattering processes. As a result, the dispersion relation for the renormalized band structure is written in Eqs. (2.4) above.

To make progress, we explicitly write the two diagrams shown in Fig. 4. The first diagram [Fig. 4(a)] represents the usual renormalized band-structure contribution to the coupling constant

$$g_{\mathbf{q}}^{a}=g_{\mathbf{q}}^{0}\frac{r_0}{V}C_r^{++}(\theta_{\mathbf{k}+\mathbf{q}},\theta_{\mathbf{k}}) , \tag{2.13a}$$

where $g_{\mathbf{q}}^{0}$ is the unscreened electron-phonon coupling constant and the angle $\theta_{\mathbf{k}}$ is defined in Eq. (2.4a). The coherence factors $C_r^{\alpha\alpha'}$, which arise from the diagonalization of the Hamiltonian, relate to the various projections on the antibonding, bonding, etc., states and are discussed in more detail in Ref. 31. As indicated by the presence of the boson propagator, the second diagram, on the other hand, includes the screening response. This diagram is expressed as

$$g_{\mathbf{q}}^{b}=g_{\mathbf{q}}^{0}\frac{r_0}{V}\sum_{r,r'}C_r^{++}(\theta_{\mathbf{k}+\mathbf{q}},\theta_{\mathbf{k}})D_{rr'}(q) \times\sum_{p,\alpha\alpha'=\pm}C_{r'}^{\alpha\alpha'}(\theta_{\mathbf{p}},\theta_{\mathbf{p}+\mathbf{q}})G_p^{\alpha}G_{p+q}^{\alpha'}N , \tag{2.13b}$$

where the noninteracting quasiparticle Greens function for the α band is $G_k^{\alpha}=(i\omega-E_k^{\alpha})^{-1}$ and the factor N comes from the summation over spin degeneracy. We use a four-momenta representation where $q=(i\omega,\mathbf{q})$.

Equation (2.13b) describes the additional screening response, via auxiliary bosons induced by a lattice distortion. The boson propagator $D_{rr'}$ in Eq. (2.13b) includes the random-phase-approximation (RPA) screening which arises from the Gaussian fluctuations about the saddle point

$$D(q)=\frac{1}{N}[\Pi_0-\Pi(q)]^{-1} , \tag{2.14a}$$

where Π_0 is the unscreened boson propagator

$$\Pi_0=\frac{2}{V^2}\begin{bmatrix} i\lambda_0 & ir_0 \\ ir_0 & 0 \end{bmatrix} \tag{2.14b}$$

and the polarization bubble diagram is given by

$$\Pi_{rr'}=-\frac{1}{\beta}\sum_{k,\alpha\alpha'=\pm}C_r^{\alpha\alpha'}(\theta_{\mathbf{k}},\theta_{\mathbf{k}+\mathbf{q}})C_{r'}^{\alpha'\alpha}(\theta_{\mathbf{k}+\mathbf{q}},\theta_{\mathbf{k}})G_k^{\alpha}G_{k+q}^{\alpha'} . \tag{2.14c}$$

The boson propagator $D_{rr'}$ is represented by a 2×2 matrix to describe two interaction channels, the hybridization and d-energy-level screening response. When Eqs. (2.14) are substituted into Eqs. (2.13), the expression for the screened coupling constant, $g_{\mathbf{q}}^{\mathrm{sc}}=g_{\mathbf{q}}^{a}+g_{\mathbf{q}}^{b}$, is easily derived

$$g_{\mathbf{q}}^{\mathrm{sc}}=g_{\mathbf{q}}^{0}\frac{r_0}{V}\left[C_r^{++}(\theta_{\mathbf{k}+\mathbf{q}},\theta_{\mathbf{k}}) +N\sum_{r,r'}C_{r'}^{++}(\theta_{\mathbf{k}+\mathbf{q}},\theta_{\mathbf{k}}) \times\left[-\frac{\delta_{rr'}}{N}+[D(q)\Pi_0]_{rr'}\right]\right] . \tag{2.15}$$

We simplify the expression in Eq. (2.15) by explicitly expressing the coherence factors $C_{\mu}^{\alpha\alpha'}$ near the metal-insulator transition. First, we categorize two screening responses which come from the r and λ channels, respectively. These are further decomposed into screening contributions from the bonding $(-)$ and antibonding $(+)$ bands. We approximate the coherence factors

$$\begin{aligned} C_r^{++}&\approx\frac{\xi_{\mathbf{k},\mathbf{q}}r_0}{(\varepsilon_d-\varepsilon_p)} , \\ C_r^{--}&\approx\frac{-2\eta_{\mathbf{k},\mathbf{q}}r_0}{\varepsilon_d-\varepsilon_p}\left[1-\frac{\xi_{\mathbf{k},\mathbf{q}}r_0^2}{4(\varepsilon_d-\varepsilon_p)^2}\right] , \\ C_r^{+-}&\approx\gamma_{\mathbf{k}}\left[\frac{(2\gamma_{\mathbf{k}+\mathbf{q}}^2+\xi_{\mathbf{k},\mathbf{q}})r_0^2}{2(\varepsilon_d-\varepsilon_p)^2}-1\right] \end{aligned} \tag{2.16a}$$

where $\xi_{\mathbf{k},\mathbf{q}}=\gamma_{\mathbf{k}+\mathbf{q}}^2+\gamma_{\mathbf{k}}^2$ and $\eta_{\mathbf{k},\mathbf{q}}=\gamma_{\mathbf{k}+\mathbf{q}}\gamma_{\mathbf{k}}$. Equation (2.16a) is derived by retaining terms up to order r_0^2. Similarly, the λ-channel coherence factors are expanded to lowest nonvanishing order,

$$\begin{aligned} C_{\lambda}^{++}&\approx i\left[1-\frac{\xi_{\mathbf{k},\mathbf{q}}r_0^2}{2(\varepsilon_d-\varepsilon_p)^2}\right], \\ C_{\lambda}^{--}&\approx\frac{-i\eta_{\mathbf{k},\mathbf{q}}r_0^2}{(\varepsilon_d-\varepsilon_p)^2} , \\ C_{\lambda}^{+-}&\approx\frac{i\gamma_{\mathbf{k}}r_0}{\varepsilon_d-\varepsilon_p} . \end{aligned} \tag{2.16b}$$

It should be stressed that Eqs. (2.16) are valid when $r_0\ll\varepsilon_d-\varepsilon_p$. Near the metal-insulator transition, this condition is satisfied because $r_0\to0$ while $\varepsilon_d-\varepsilon_p$ ap-

proaches a constant. When the doping concentration becomes larger, however, the expansion will not be simple since higher-order terms in r_0 will no longer be negligible.

The polarization bubble diagrams for each channel are simplified by inserting Eqs. (2.16) into Eq. (2.14c). The rr-channel bubble diagram (up to a lowest order in r_0^2) is written as

$$\Pi_{rr}(q)\approx\sum_{\mathbf{k}}\left[\bar{\chi}_{\mathbf{k},\mathbf{q}}+\frac{r_0^2}{(\varepsilon_d-\varepsilon_p)^2}[\xi_{\mathbf{k},\mathbf{q}}^2\chi_{\mathbf{k},\mathbf{q}}^{++}-2\eta_{\mathbf{k},\mathbf{q}}^2(\chi_{\mathbf{k},\mathbf{q}}^{+-}+\chi_{\mathbf{k},\mathbf{q}}^{-+})-\xi_{\mathbf{k},\mathbf{q}}\bar{\chi}_{\mathbf{k},\mathbf{q}}+4\eta_{\mathbf{k},\mathbf{q}}^2\chi_{\mathbf{k},\mathbf{q}}^{--}]\right], \tag{2.17a}$$

where

$$\chi_{\mathbf{k},\mathbf{q}}^{\alpha\alpha'}=-\frac{1}{\beta}\sum_{i,\omega}G_{k+q}^{\alpha}G_k^{\alpha'},$$

and

$$\bar{\chi}_{\mathbf{k},\mathbf{q}}=\gamma_{\mathbf{k}}^2\chi_{\mathbf{k},\mathbf{q}}^{+-}+\gamma_{\mathbf{k}+\mathbf{q}}^2\chi_{\mathbf{k},\mathbf{q}}^{-+}.$$

The contribution from the $r\lambda$ channel is identical to the λr channel and found to be linearly proportional to r_0

$$\Pi_{\lambda r}(q)\approx\frac{ir_0}{(\varepsilon_d-\varepsilon_p)}\sum_{\mathbf{k}}(\xi_{\mathbf{k},\mathbf{q}}\chi_{\mathbf{k},\mathbf{q}}^{++}-\bar{\chi}_{\mathbf{k},\mathbf{q}}). \tag{2.17b}$$

Finally, the $\lambda\lambda$-channel bubble diagram is written as

$$\Pi_{\lambda\lambda}(q)\approx-\sum_{\mathbf{k}}\left[\chi_{\mathbf{k},\mathbf{q}}^{++}+\frac{r_0^2}{(\varepsilon_d-\varepsilon_p)^2}(\bar{\chi}_{\mathbf{k},\mathbf{q}}-\xi_{\mathbf{k},\mathbf{q}}\chi_{\mathbf{k},\mathbf{q}}^{++})\right]. \tag{2.17c}$$

When these diagrams are explicitly evaluated, the internal degrees of freedom k in the polarization bubble must summed. However, since we are only interested in qualitative behavior here, we do not explicitly perform this summation.

Collecting together all contributions by substituting Eqs. (2.16) and (2.17) into Eq. (2.15), we obtain the screened electron-phonon coupling constant

$$g_{\mathbf{q}}^{\mathrm{sc}}=g_{\mathbf{q}}^0\frac{2r_0^2}{V^3\det(\Pi_0-\Pi)}\times\left[\frac{\lambda_0\xi_{\mathbf{k},\mathbf{q}}}{\varepsilon_d-\varepsilon_p}\sum_{\mathbf{k}'}\chi_{\mathbf{k}',\mathbf{q}}^{++}+\sum_{\mathbf{k}'}\bar{\chi}_{\mathbf{k}',\mathbf{q}}-\frac{2\lambda_0}{V^2}\right]. \tag{2.18}$$

As deduced in the frozen-phonon approach, this coupling constant varies as r_0^2 near the half-filled limit. This behavior represents the dramatic screening of the electron-phonon interactions by Coulomb correlations (since $r_0\to0$ as $x\to0$), which we have found in our earlier approach. However, well away from the metal-insulator transition, the simple expression we have derived is not valid. Higher-order correction terms such as $O(r_0^4)$ must be added since they are no longer negligible.

III. IMPLICATION FOR TRANSPORT PROPERTIES

A. Formalism

The temperature-dependent resistivity ρ in the metallic copper oxides has received considerable attention because of its ubiquitous linear behavior.[6,12] Furthermore, on the basis of anisotropy in the resistivity, Anderson has conjectured that the cuprates are sufficiently two dimensional so that they cannot exist in a Fermi-liquid state. Recently, however, in $YBa_2Cu_3O_{7-\delta}$, a metalliclike resistivity for both directions along and perpendicular to the copper-oxygen plane has been claimed.[32] At this stage, however, the experimental situation is uncertain as is the appropriateness of a Fermi-liquid approach. In this section we address the resistivity and its two components, the transport mass m^*/n and the lifetime τ, using our Fermi-liquid approach applied to the electron-phonon system.

By solving the linearized transport equation we may express the resistivity as

$$\rho=\frac{m^*}{ne^2}\frac{1}{\tau}. \tag{3.1}$$

The transport mass is easily evaluated

$$\frac{m^*}{n}=\frac{1}{\sum_{\mathbf{k}}(v_{k_a}v_{k_b})\delta(E_{\mathbf{k}}-E_F)}. \tag{3.2}$$

Here, $v_{k_a}=\partial E_{\mathbf{k}}/\partial k_\alpha$ is the $\alpha=x,y,z$ component of the quasiparticle velocity. When a parabolic dispersion is used in Eq. (3.2), the free-electron value is recovered. However, for a tight-binding band structure such as ours, m^*/n is more complicated and contains enhancement due to Coulomb effects. The magnitude of these enhancements may be estimated as $m^*/n\propto1/[v_F^2N(E_F)]\propto e_0^2$. Correlation effects, therefore, yield a diverging transport mass as the metal-insulator transition is approached (i.e., $m^*/n\to\infty$ as $e_0\to0$), which is expected from Mott localization.

Correlation effects on the transport lifetime, on the other hand, are more difficult to calculate. In general, the lifetime arises from a multiplicity of scattering sources such as electron-electron, magnetic, and electron-phonon interactions. If the copper oxides resemble typical metals in any way, then the electron-phonon scattering contribution should not be ignored. Furthermore, characterizing this contribution will allow us to determine the nature of other scattering mechanisms which are present. We, therefore, discuss the electron-phonon contribution to the transport lifetime using the results of Sec. II. By solving the Boltzmann transport equation variationally, we write the lifetime from electron-phonon interactions as

$$\frac{1}{\tau_{\rm ph}}=\frac{2\pi}{k_B T}\int d\varepsilon\, d\varepsilon'\, d\omega\, \alpha^2_{\rm tr}F(\omega,\varepsilon,\varepsilon')f_\varepsilon(1-f_{\varepsilon'}) \times[(n_\omega+1)\delta(\varepsilon-\varepsilon'-\omega) +n_\omega\delta(\varepsilon-\varepsilon'+\omega)]\ , \tag{3.3}$$

where f_ε and n_ω are the Fermi and Bose function, respectively. Here, the energies ε are measured with respect to E_F. In Eq. (3.3), the details of the electron-phonon interaction and correlation effects are contained in the transport spectral function

$$\alpha^2_{\rm tr}F(\omega,\varepsilon,\varepsilon')=N(E_F)\frac{\sum_{\mathbf{k},\mathbf{k}'}(v_{k_x}-v_{k_x'})^2|g_{\mathbf{q},\nu}|^2\delta(E_{\mathbf{k}}-\varepsilon)\delta(E_{\mathbf{k}'}-\varepsilon')\delta(\omega-\omega_{\mathbf{q},\nu})}{2\sum_{\mathbf{k},\mathbf{k}'}v^2_{k_x}\delta(E_{\mathbf{k}})\delta(E_{\mathbf{k}'})}\ , \tag{3.4}$$

where the phonon wave vector is $\mathbf{q}=\mathbf{k}'-\mathbf{k}$. The contribution from the quasiparticle velocity which vanishes as the insulator is approached is partially canceled by correlation effects from two competing sources: the density of states $N(E_F)$ which diverge as $x\to 0$, and the electron-phonon matrix element $g_{\mathbf{q},\nu}$, which vanishes as shown in Sec. II.

We evaluate Eq. (3.3) using some fairly standard approximations. We assume that $\alpha^2_{\rm tr}F(\omega,\varepsilon,\varepsilon')$ is independent of ε. This approximation is valid when the bandwidth is much larger than either k_BT and $\omega_{\mathbf{q},\nu}$. When the integration over ε and ε' is performed, the scattering rate is written as

$$\frac{1}{\tau_{\rm ph}}=4\pi k_B T\int_0^\infty d\omega\frac{\alpha^2_{\rm tr}F(\omega)}{\omega}Q(x)\ , \qquad Q(x)=\left[\frac{x}{\sinh x}\right]^2\ , \tag{3.5}$$

where $x=\omega/2k_BT$ and ω is a phonon frequency. Equation (3.5) varies as $1/\tau_{\rm ph}\propto T$ at high temperatures and becomes $1/\tau_{\rm ph}\propto T^5$ at low temperatures. This crossover temperature is of the order of $\frac{1}{4}$ the characteristic phonon frequency. In general, however, there is a range of phonon frequencies, which will lead to a more complicated T dependence.

The entire electron-phonon picture breaks down if either the thermal, k_BT, or Debye energy, ω_D, becomes comparable to the bandwidth. In our renormalized band-structure picture, this occurs at low concentrations close to the metal-insulator transition, since then the bandwidth is significantly reduced by incipient localization. To quantify this point, we plot, in Fig. 5 (where we define $\beta=t/V$), the bandwidth as a function of doping concentration and compare it with the phonon density of states for $La_{1.85}Sr_{0.15}CuO_4$.[33] For definiteness, we use the parameters $V=1.6$ eV with $t=0.4$ (circles) and 0.8 eV (triangles). As shown in the figure, for $x\approx 0.05$ the bandwidth is only marginally larger than the Debye energy. However, as the doping concentration grows larger, the *adiabatic* approximation is more appropriate. Because the intrinsic oxygen bandwidth increases with oxygen-oxygen hopping, this approximation may be extended to somewhat lower x with inclusion of oxygen-oxygen overlap integrals.

Evaluating Eq. (3.4) exactly is difficult because $\alpha^2_{\rm tr}F(\omega)$ involves the average over phonon wave vectors $\mathbf{q}$ as well as the summation over electron wave vectors $\mathbf{k}$. Therefore, we need to make further (standard) approximations. For the average over $\mathbf{q}$, we sample only at few chosen wave vectors to reproduce the spectral function reliably. Because there is more phase space for large vectors, we primarily sample wave vectors near the zone edge. In simplifying the summation over $\mathbf{k}$, we use the conservation relations to rewrite the δ function in Eq. (3.4)

$$\delta(E_{\mathbf{k}}-\varepsilon)\delta(E_{\mathbf{k}'}-\varepsilon')\delta(\omega-\omega_{\mathbf{q},\nu}) \to\delta(E_{\mathbf{k}'}-E_{\mathbf{k}}-\omega_{\mathbf{q},\nu})+\delta(E_{\mathbf{k}'}-E_{\mathbf{k}}+\omega_{\mathbf{q},\nu})\ . \tag{3.6}$$

Based on Eq. (3.6) and the assumption that the Fermi surface does not change significantly within ω_D, we may replace the complicated $\mathbf{k}$ summation with a Fermi surface (fs) average,[34] $\overline{g^2_{\mathbf{q},\nu}}$,

$$\overline{g^2_{\mathbf{q},\nu}}=\frac{\langle\langle(v_{k_x}-v_{k_x'})^2|g_{\mathbf{q},\nu}|^2\rangle\rangle_{\rm FS}}{\langle\langle(v_{k_x}-v_{k_x'})^2\rangle\rangle_{\rm FS}}\ . \tag{3.7}$$

We evaluate Eq. (3.7) numerically using the expression

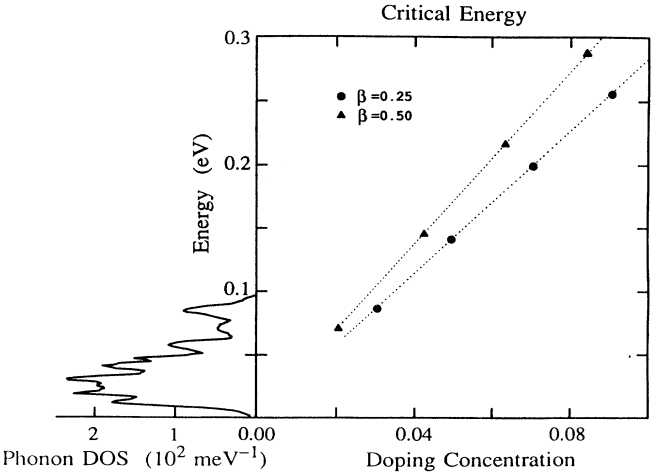

FIG. 5. The bandwidth of the antibonding band as a function of doping concentration compared with the phonon density of states (DOS) from Ref. 33. This shows the range of validity of adiabatic approximation.

for the transition matrix element $g_{\mathbf{q},\nu}$ from Appendix B. This leads to the quantity $K(\omega)=\alpha^2_{\rm tr}F(\omega)/\omega$,

$$K(\omega_{\mathbf{q},\nu})\approx\frac{N(E_F)}{M_{\mathbf{q},\nu}\omega^2_{\mathbf{q},\nu}N_{\rm cell}}\frac{\langle\langle(v_{k_x}-v_{k_x'})^2\rangle\rangle_{\rm FS}}{2\langle\langle v^2_{k_x}\rangle\rangle_{\rm FS}}\overline{g^2_{\mathbf{q},\nu}}. \tag{3.8}$$

This function will, in general, be dominated by phonons of low characteristic frequency. It is furthermore enhanced by quasinesting effects arising from the strong coupling of the zone edge phonon $\mathbf{X}(\frac{1}{2},\frac{1}{2},0)$. Simple power counting arguments show that, as the insulator is approached, $K\propto e_0^2$. This has, as an important implication, the fact that the resistivity ρ from electron-phonon interactions is essentially independent of doping concentration. This is a consequence of the divergence of the transport mass and the vanishing of the inverse lifetime, or alternatively, $K(\omega)$.

B. Numerical results and comparison with experiment

In this section we discuss the results of our numerical calculation of the transport properties and compare them with a variety of experiments. We use the band-structure model of Eq. (2.1) which includes both direct oxygen-oxygen hopping processes as well as copper-oxygen hybridization. For notational simplicity we define the two-dimensionless parameters

$$\alpha=V/(\varepsilon_p-\varepsilon_d^0)$$

and

$$\beta=t/V\ ,$$

where V is the nearest-neighbor copper-oxygen hopping integral and t is the oxygen-oxygen overlap matrix element. For definiteness, we use the parameters $\varepsilon_p-\varepsilon_d^0=4.0$ eV and $V=1.6$ eV, as cited in the literature. Throughout this section we assume that the Coulomb correlation on a copper site is infinite and take the two values $t=0.4$ and 0.8 eV to illustrate the effect of varying the oxygen-oxygen overlap integrals.

In Fig. 6, we plot the concentration dependence of the transport mass as determined from Eq. (3.2). For definiteness we choose $\beta=0.5$. As illustrated in the figure, the transport mass changes dramatically with x near the metal-insulator transition and m^*/n varies qualitatively as $1/x$ with small x. Because the carrier density is close to one, it is clear, within our formalism, that a divergence of the transport mass is a consequence of Brinkman-Rice or Mott localization (and not of a small carrier number n). In the figure, the transport mass, at $x=0.3$, is enhanced roughly by four times that of the free-electron mass and it depends weakly on x. At $x\approx0.06$, the effective mass is almost 20 times the electron mass. In Fig. 6 there is also a small cusp arising from a van Hove singularity. As shown in Ref. 9, when oxygen-oxygen terms are introduced, the van Hove singularity is shifted from its symmetrical position in the density of states $N(E)$ so that it overlaps E_F at around $x=0.15$.

The calculated plasma frequency ω_P may be compared with that measured in infrared experiments.[35,36] We plot, in Fig. 7, ω_P as a function of x. Although we choose $\beta=0.25$ in this figure, other values of β lead to similar results, both in the magnitude and x dependence. Because the inverse of the transport mass is related to the plasma frequency by $\omega_P^2=4\pi e^2n/m^*$, ω_P varies roughly as $x^{1/2}$ with x. It should be noted that this x dependence is consistent with optical data summarized in Fig. 1(a) for both $La_{2-x}Sr_xCuO_4$ and $YBa_2Cu_3O_{7-\delta}$. As shown in Fig. 7, our localization theory predicts $\omega_p\approx0.8$ eV for $x>0.25$, whereas the observed value is roughly 1.0 eV in $La_{2-x}Sr_xCuO_4$ (Refs. 13 and 35) and it ranges from 0.8 to 3.0 eV in $YBa_2Cu_3O_{7-\delta}$.[35,36,16]

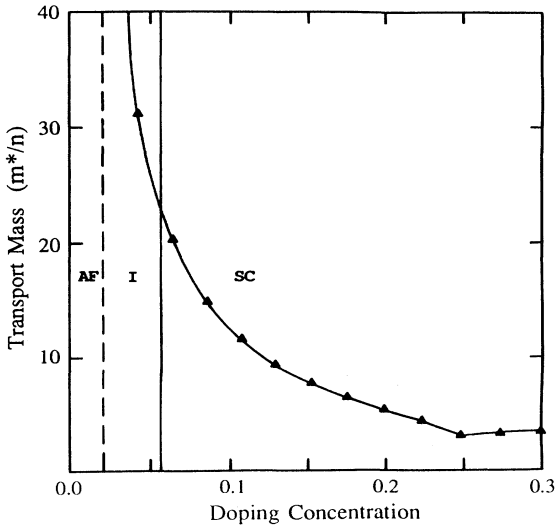

FIG. 6. Concentration dependence of the transport mass for $\beta=0.50$. The small kink reflects the van Hove singularity.

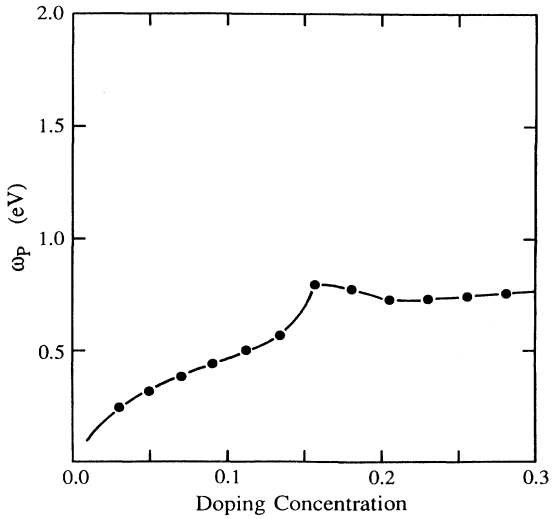

FIG. 7. Concentration dependence of the plasma frequency for $\beta=0.25$. See Fig. 1(a) for a comparison with experiment.

In Fig. 8, the electron-phonon transport spectral function is plotted for $\beta=0.25$ and $x=0.15$. In evaluating Eq. (3.4), we use the frequencies estimated by Cohen *et al.* from their lattice-dynamics calculation[26] for the zone edge modes and the matrix elements from the frozen-phonon method of Sec. II A. In the inset, we compare the phonon density of states $F(\omega)$ data on $La_{1.85}Sr_{0.15}CuO_4$ with that obtained from the lattice-dynamics calculation (shaded histogram). As illustrated in the figure, the calculated $F(\omega)$ qualitatively reproduces the general features of the experimental results. The differences in the characteristic frequencies presumably are due to screening effects which are not fully accounted for by LDA calculations. For the most part, the higher (oxygen) frequencies are overestimated while the lower (copper) frequencies are underestimated. A similar comparison can be inferred from reflectivity data.[36,37] Although incorporation of these differences would lead to some changes in the calculated α^2F, the qualitative features remain unchanged. A rough fit to our spectral function yields a double-peak structure with each peak associated with a predominantly Cu-like or O-like modes. Because the higher-frequency oxygen modes, which tend to induce a static charge-density wave (CDW) have a larger coupling constant than the copper modes, the amplitudes of the spectral function for $\omega<70$ meV are smaller than those for $\omega>70$ meV. As we might expect, the amplitude from transverse motion is almost negligible.

In Fig. 9, we plot the temperature-dependent resistivity ρ as calculated from Eq. (4.9). The solid curve is that obtained using our microscopically derived $\alpha^2_{tr}F(\omega)$ with the frequency spectrum calculated by Cohen and coworkers.[26] Although this curve is close to linear and linearity extends down to low temperatures, it is not precisely linear. A linear resistivity at low temperatures derives from low-frequency phonons which, in the present case, can be attributed to the low-lying copper modes. (These modes should not be confused with orthorhombic distortions which do *not* couple strongly to the electrons.) A close examination of the solid curve reveals that there is a slight change in slope of resistivity at 150 K. This is the consequence of the double-peak spectral function shown in Fig. 8.

A similar calculation may be performed for a more phenomenologically derived phonon spectrum where the frequencies better match those measured in neutron and infrared experiments. We indicate the results for the resistivity by the dashed curve of Fig. 9. In this calculation, we associate the lowest-frequency copper mode with 12 meV (instead of 6 meV of Ref. 26), and the highest-frequency oxygen mode with 90 meV (instead of 140 meV of Ref. 26). Then we rescale all the frequencies between the two extremes and put additional weight, as is indicated by $F(\omega)$ data, on the copper modes. Even for this modified spectrum, there are only small changes in the resistivity curve.

To avoid uncertainties from impurities and lattice defects, we plot the slope $d\rho/dT$ of the resistivity as a function of x in Fig. 10. By way of summary, we show the data on $La_{2-x}Sr_xCuO_4$ at 300 K taken by several groups in different symbols (squares,[37] triangles,[38] crosses,[39] and circles[17]). With the exception of the triangles, all of the

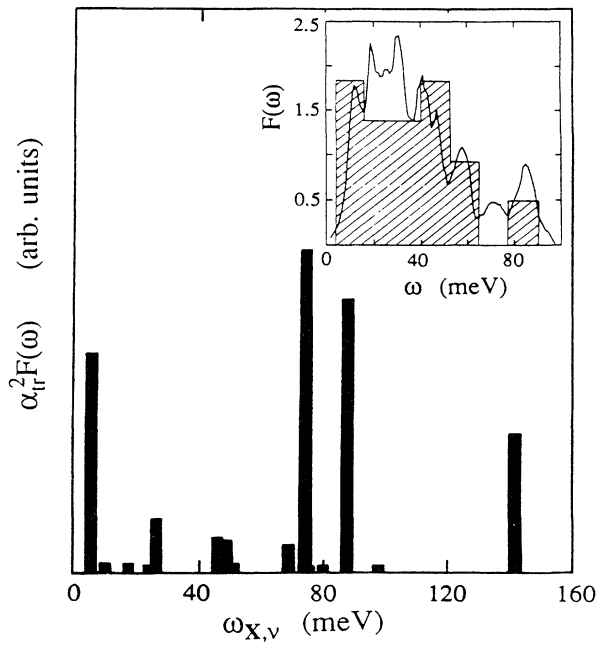

FIG. 8. Electron-phonon transport spectral function for $\beta=0.25$ and $x=0.15$. In the inset, the phonon density of states from Ref. 33 is plotted to compare with the results obtained from rescaling (see text) the lattice-dynamics calculation (shaded region) of Ref. 26.

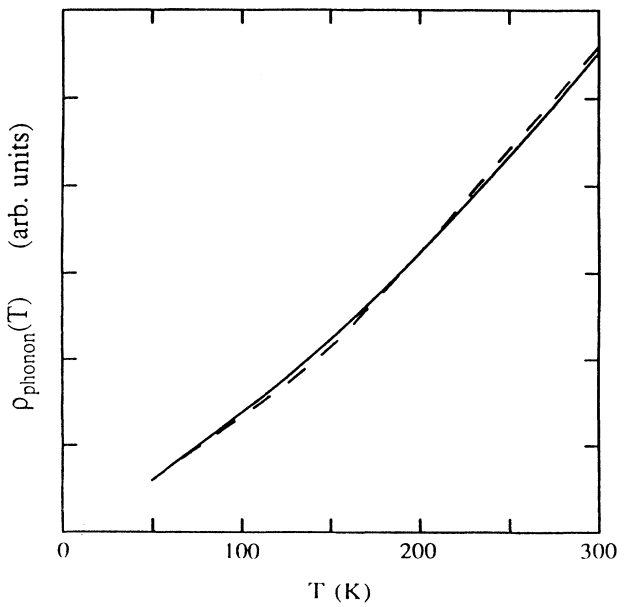

FIG. 9. Temperature-dependent resistivity at $x=0.2$ calculated from the microscopically (solid line) and phenomenologically (dashed line) derived phonon spectral function.

data are obtained from polycrystalline samples. The data from an epitaxially grown single-crystal film are denoted by triangles. Although these data are widely dispersed, there is a clear trend in x: the slope is almost independent of x for $x > 0.15$, but increases as the insulator is approached. (This behavior is not as pronounced in $YBa_2Cu_3O_{7-\delta}$ samples, perhaps, as a consequence of the copper-oxygen chains. Furthermore, the resistivity slopes do not appear to be as large in this system.) To summarize the data, we plot the dotted lines as an estimated average curve. To compare the theoretical result for $d\rho/dT$ with the data, the calculated electron-phonon contribution is indicated by the solid curve. Here we choose $\beta=0.50$. As shown in the figure, the x dependence of the slope is very weak as a result of the vanishing electron-phonon scattering rate and the diverging transport mass as $x \rightarrow 0$. This is consistent with the data in the metallic regime, but it is inconsistent near the insulator. Therefore, electron-phonon interactions alone cannot explain the data for $d\rho/dT$ for $x < 0.15$. This failure strongly implies that there are other mechanisms such as electron-electron or magnetic scattering which may be more important than electron-phonon interactions near the insulating limit.

We may obtain insight into these other scattering mechanisms phenomenologically by fitting the dotted line. We add to the electron-phonon lifetime an additional scattering time which is assumed to correspond to a concentration-independent matrix element. It follows from a Golden Rule calculation that $1/\tau_0 \propto N(E_F)T$. The size of this phenomenologically derived correction, $1/\tau_0 \approx 3.5$ meV for $x > 0.17$, is smaller than $1/\tau_{ph}$. However, as the insulator is approached, $1/\tau_0$ becomes progressively more important because of the increasingly large $N(E_F)$ arising from the narrow band and the suppression of the electron-phonon interaction.

In Fig. 11, we plot the concentration-dependent lifetime, τ, derived from electron-phonon interactions for $\beta=0.25$. We also compare the results from the phenomenological calculation in which the net τ is derived by fitting $d\rho/dT$. According to Mattiessen's rule,[40] which states that the scattering rate from various sources is additive, the lifetime will be readily dominated by the presence of other scattering mechanisms for small x. As illustrated in the figure, when $1/\tau_0$ is added to $1/\tau_{ph}$, the net τ becomes almost concentration independent. It is important to stress that this is consistent with the data plotted in Fig. 1(b).

The mean free path, $l = v_F\tau$, of a quasiparticle is plotted in Fig. 12. Here we show the calculated result as a function of concentration at 300 K for $\beta=0.25$ (circles) and 0.5 (triangles) in units of the copper-oxygen bond length, $R_{Cu\text{-}O}$. As noted before, the kinks in this figure reflect the van Hove singularities. We also plot (dotted line) the phenomenological result derived from adding $1/\tau_0$ to the electron-phonon background for $\beta=0.5$ in the dotted line. The Mott-Ioffe-Regel (MIR) condition[19] is shown by the dashed line. The calculated mean free path l_{ph} from electron-phonon interactions, in Fig. 12, shows that it is surprisingly close to the MIR limit, but it is still on the metallic side. We find l_{ph} ranges from three to eight times the bond length. This small value of l_{ph} is consistent with the data in both $La_{2-x}Sr_xCuO_4$ and $YBa_2Cu_3O_{7-\delta}$.[12] It should be stressed that the mean free path in the copper oxides is significantly shorter than in

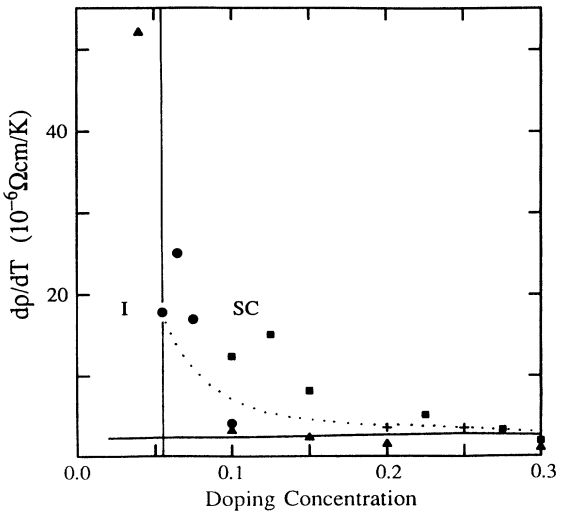

FIG. 10. Concentration dependence of the resistivity slope at 300 K. Theoretical results with (or without) a small phenomenologically added lifetime plotted by the dotted line (or solid line). The data represented by triangles, circles, squares, and crosses are from Refs. 38, 17, 37, and 39, respectively.

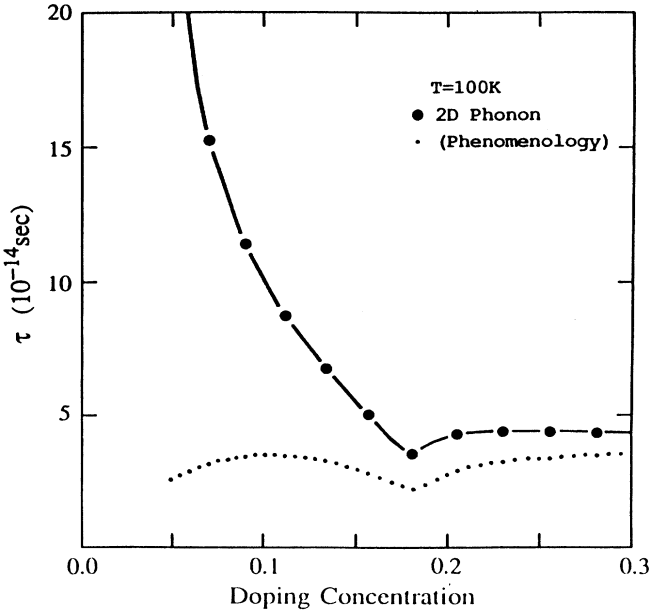

FIG. 11. Concentration dependence of the transport lifetime at 100 K and $\beta=0.25$ with (or without) a small phenomenologically added lifetime as shown by the dotted (or solid) line. See Fig. 1(b) for a comparison with experiment.

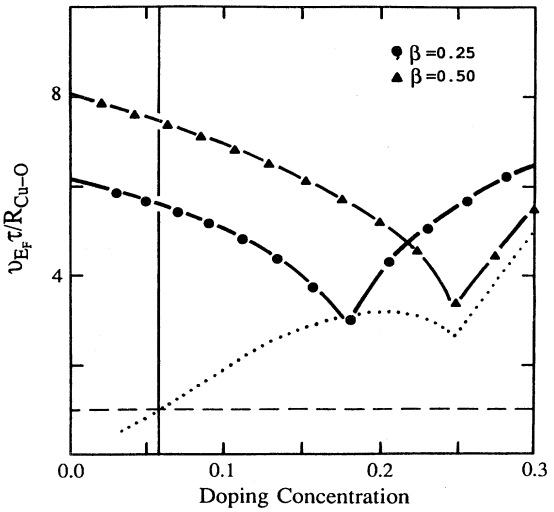

FIG. 12. Concentration dependence of the mean free path at 300 K from electron-phonon interactions for $\beta=0.25$ (circles) and 0.50 (triangles). The dotted line is obtained from adding a small phenomenological lifetime to the case $\beta=0.50$ as in Fig. 11. The dashed line represents the Mott-Ioffe-Regel condition. The dotted and MIR lines intersect at the metal-insulator transition.

copper metal where l is almost 200 times the lattice constant.[12]

The MIR line separates the metallic conductivity from insulating behavior. If the mean free path is below this value, the Boltzmann transport formalism breaks down. In this way, the metal-insulator transition in the copper oxides can be understood. The phenomenologically derived mean free path shown by the dotted line becomes shorter and shorter as the insulator is approached. Finally, it becomes comparable to the copper-oxygen bond length at $x\approx 0.05$. At the critical concentration, the system becomes insulating.

IV. CONCLUSIONS

The main contribution of the present paper has been to study the effect of very strong Coulomb correlations on electron-phonon interactions and the implications for transport properties. We have used a Fermi-liquid approach in which both a semirealistic band-structure and Brinkman-Rice or Mott localization at the half-filled limit are included. (While we have considered the "electron picture" here, our results apply to the "hole picture" for those parameters which lead to an insulating half-filled limit[31]). Although there have been previous attempts to study electron-phonon interactions in the copper oxides by using weak Coulomb correlation approaches, these schemes fail to include both of these effects simultaneously. Based on our analysis of the electron-phonon coupling, using both a frozen-phonon scheme and auxiliary boson formalism, we argued that Coulomb correlations tend to suppress charge fluctuations within the copper-oxygen plane, thereby reducing the electron-phonon coupling constant as the metal-insulator transition is approached. As a result, we are able to reconcile the calculated electron-phonon contribution to $d\rho/dT$ with the necessarily larger measured slope. We stress that, as the quality of data improves, $d\rho/dT$ appears to decrease so that this poses an even more severe upper bound on the electron-phonon coupling.

As a consequence of Mott localization, we have shown that the transport mass m^*/n diverges as the insulator is approached. This is consistent with the concentration-dependent plasma frequency, $\omega_P^2 \propto x$ as found in both $La_{2-x}Sr_xCuO_4$ and $YBa_2Cu_3O_{7-\delta}$. It should be stressed that we cannot distinguish the appropriateness of either $m^* \propto 1/x$ or $n \propto x$ approaches from these plasma data. In the electron-phonon contribution to the resistivity $\rho \propto (m^*/n)(1/\tau_{ph})$, because electron-phonon coupling becomes weak as $x \rightarrow 0$, two competing correlation effects are canceled. Therefore, the electron-phonon contribution to the resistivity becomes almost concentration independent. A temperature-dependent analysis of this component of the resistivity shows that, due to the presence of a high density of low-frequency copperlike modes, this ρ is quasilinear down to roughly 50 K.

In this paper, we have not addressed other scattering mechanisms such as electron-electron or magnetic interactions, but the present theory has demonstrated they become more important as the insulator is approached. While the electron-phonon contribution to the resistivity slope accounts for most of the observed value in the metallic regime ($x > 0.15$), it becomes progressively less important as the metal-insulator transition is approached ($x < 0.15$). This suggests that other scattering mechanisms would be more important than phonons at small hole doping. In order to fit the data, we have added a phenomenological lifetime of the form $1/\tau_0 \propto N(E_F)T$ to the phonon background. As a result, we found that the overall scattering rate becomes almost concentration independent, and this is consistent with the x independent lifetime inferred from the Drude conductivity. The microscopic basis for $1/\tau_0$ cannot be ascertained because a linear T dependence is a general consequence of scattering from bosons with low characteristic frequencies, when the temperature is higher than $\frac{1}{4}$ of the characteristic boson energy.[41]

Based on mean-free-path calculations, we have argued that the doped copper oxides are poor metals, in contrast to transition or noble metals such as Cu, because they are on the verge of satisfying the Mott-Ioffe-Regel criterion. For concentrations less than $x = 0.05-0.07$, we would predict a transition to insulating behavior as is observed experimentally.

Finally, we note that the upper bound on λ imposed by the resistivity data above (in conjunction with ac conductivity Drude fits) makes it difficult to understand how a purely phonon-driven superconducting mechanism could lead to high transition temperatures. More elaborate scenarios may be proposed which yield strong coupling in the superconducting "channel" and weak phonon scattering in the transport "channel." One contribution of the present work is to underline the importance of considering the constraints imposed on the electron-phonon coupling which arise from ac and dc conductivity measure-

ments. Clearly, in future proposals for superconducting mechanisms these constraints must be considered.

ACKNOWLEDGMENTS

We thank G. Thomas for providing us with his data prior to publication. Useful conversations with T. F. Rosenbaum and S. Nagel are acknowledged. This work was supported by NSF-STC Grant No. STC-8809854, NSF-MRL Grant No. DMR-16892US, DOE Grant Nos. DE-AC02-76H00016 and NSF-DMR-8914045. A.A. acknowledges the Alfred P. Sloan Foundation for support.

APPENDIX A: 1D ELECTRON-PHONON TRANSITION MATRIX ELEMENTS

In this section, we focus on a simplified one-dimensional (copper-oxygen chain) model for the purpose of obtaining insight into the electron-phonon interaction in the copper oxides. Even with this simple model, solving the self-consistent equations as described in Ref. 9 for an arbitrary phonon wave vector is difficult. We, therefore, simplify the calculation further by considering only phonon modes that are most relevant to transport properties. For instance, the zone edge ($\mathbf{q}=\mathbf{X}$) phonon modes, identical to the Periels distortion, interact strongly with electrons by way of doubling the unit cell, (i.e., by Brillouin zone folding). Therefore, phonon modes with this wave vector are important for transport. The zone center ($\mathbf{q}=\Gamma$) modes, on the other hand, are more relevant for Raman scattering and less important for transport measurements. There are six $\mathbf{X}$ modes in one dimension, two of which are longitudinal (the oxygen and copper breathing modes), the remaining four are twofold-degenerate transverse modes. For simplicity, we classify them into three types by considering the oxygen and copper breathing modes as distinct since they involve rather different electronic responses.

To calculate the renormalized band-structure and the quasiparticle states in the infinite U_d limit, we may apply a slave boson formalism to a distorted ($\mathbf{X}$ mode) lattice. Within this approach, we extend the Anderson lattice Hamiltonian, discussed in Ref. 9,

$$H_{\mathrm{FP}}^{1d}=\sum_{i,\sigma}\left[\sum_{n}\varepsilon_{d,n}^{0}d_{in\sigma}^{\dagger}d_{in\sigma}+\sum_{m}\varepsilon_{p,m}C_{im\sigma}^{\dagger}C_{im\sigma}+\sum_{\langle nm\rangle}V_{n,m}(d_{in\sigma}^{\dagger}\mathbf{e}_{in}C_{im\sigma}+C_{im\sigma}^{\dagger}\mathbf{e}_{in}^{\dagger}d_{in\sigma})\right], \tag{A1}$$

where the indices n and $m=1,2$ denote two positions for the copper and oxygen orbitals, respectively, and $\langle nm\rangle$ denotes the pairs of nearest-neighbor copper-oxygen orbitals. The operators $\mathbf{e}_{in}^{\dagger}$ and $d_{in\sigma}^{\dagger}$ create Cu^{3+} and Cu^{2+} states, respectively, whereas $C_{im}^{\dagger}$ creates an electron at the mth oxygen site. Here, each phonon mode is characterized by the relative displacements of copper and oxygen ions. Equation (2.6) is imposed on each copper site. Except for the states near $k_{ZE}=\pm\pi/2a$, the renormalized band structure obtained from a solution of the mean-field equations for H_{FP}^{1d} is similar to that obtained by folding the BZ of the undistorted lattice. We may express this band structure in terms of the $\theta_{\mathbf{k}}$ function defined by Eq. (2.4a), but with $\gamma_{\mathbf{k}}=2\cos(ka/2)$ instead of Eq. (2.4b). The quasiparticle operator $\Phi_{k,\sigma}$ of the Hamiltonian is easily expressed as a linear combination of copper and oxygen orbitals at different sites. We may write this in terms of a unitary matrix $\mathbf{U}$

$$\Phi_{k,\sigma}=\begin{bmatrix}\alpha_{k,\sigma}\\ \alpha_{k+Q,\sigma}\\ \beta_{k,\sigma}\\ \beta_{k+Q,\sigma}\end{bmatrix}=\frac{1}{\sqrt{2}}\begin{bmatrix}\sin\theta_k & \sin\theta_{k+Q} & i\cos\theta_{k+Q} & \cos\theta_k\\ \sin\theta_k & -\sin\theta_{k+Q} & -i\cos\theta_{k+Q} & \cos\theta_k\\ \cos\theta_k & i\cos\theta_{k+Q} & \sin\theta_{k+Q} & -\sin\theta_k\\ \cos\theta_k & -i\cos\theta_{k+Q} & -\sin\theta_{k+Q} & -\sin\theta_k\end{bmatrix}\begin{bmatrix}d_{1,k,\sigma}\\ d_{2,k,\sigma}\\ C_{1,k,\sigma}\\ C_{2,k,\sigma}\end{bmatrix}, \tag{A2}$$

where $Q=\pi/a$ denotes the wave vector for a frozen-phonon mode. Here, α and β destroy quasiparticles in the antibonding and bonding bands, respectively.

Although the states at k_{BZ} are degenerate as a consequence of BZ folding, this degeneracy is lifted by ionic displacements because a distortion changes the renormalized parameters ε_d and r_n. The electron-phonon Hamiltonian, therefore, is given by Eq. (2.8) with the distortion matrix $\overline{\mathbf{M}}_D$,

$$\overline{\mathbf{M}}_D=\mathbf{U}\cdot\mathbf{M}_D\cdot\mathbf{U}^{\dagger} \tag{A3}$$

and

$$\mathbf{M}_D=\begin{bmatrix}\varepsilon_{d,1}-\varepsilon_d & 0 & (r_1e^{i\mathbf{k}\cdot\delta\mathbf{R}}-r_0)e^{-i\tilde{k}} & (r_1e^{-i\mathbf{k}\cdot\delta\mathbf{R}}-r_0)e^{i\tilde{k}}\\ 0 & \varepsilon_{d,2}-\varepsilon_d & (r_2e^{i\mathbf{k}\cdot\delta\mathbf{R}}-r_0)e^{i\tilde{k}} & (r_2e^{-i\mathbf{k}\cdot\delta\mathbf{R}}-r_0)e^{-i\tilde{k}}\\ (r_1e^{-i\mathbf{k}\cdot\delta\mathbf{R}}-r_0)e^{i\tilde{k}} & (r_2e^{-i\mathbf{k}\cdot\delta\mathbf{R}}-r_0)e^{-i\tilde{k}} & \varepsilon_{p,1}-\varepsilon_p & 0\\ (r_1e^{i\mathbf{k}\cdot\delta\mathbf{R}}-r_0)e^{-i\tilde{k}} & (r_2e^{i\mathbf{k}\cdot\delta\mathbf{R}}-r_0)e^{i\tilde{k}} & 0 & \varepsilon_{p,2}-\varepsilon_p\end{bmatrix},$$

where δR is the displacement vector (for either copper or oxygen ions) and $\tilde{k}=ka/2$. The renormalized copper level and effective hybridization are $\varepsilon_{d,n}=\varepsilon^0_{d,n}+\lambda_n$ and $r_n=e_n V(R\pm\delta R)$. There are two contributions to the matrix $\mathbf{M}_D$ which ultimately lead to electron-phonon scattering processes: one is the shift in Bloch waves by a lattice distortion and other is the change in electronic potential brought about by band renormalizations. The latter contribution is simplified as follows. We assume that the bare energy levels for copper sites are identical. (The results do not change significantly even when this restriction is relaxed. As a consequence of screening, the energy-level difference, $\varepsilon^0_{d,1}-\varepsilon^0_{d,2}$, between the copper sites is mostly canceled by the quantity $\lambda_1-\lambda_2$ because Coulomb renormalizations tend to minimize the effects of an external perturbation by acting as a restoring force.) Similarly, we extend this approximation to the oxygen sites (i.e., $\varepsilon^0_{d,1}=\varepsilon^0_{d,2}=\varepsilon^0_d$ and $\varepsilon_{p,1}=\varepsilon_{p,2}=\varepsilon_p$).

In order to evaluate Eq. (2.10b), we need to account for the variational response functions in Eq. (2.12). We distinguish these functions by their origin. For instance, the hybridization screening response is brought about by either copper or oxygen motion which changes the copper-oxygen overlap integral. As shown in Ref. 29, the variational response of copper, $S_{\mathrm{Cu}}=V(\delta e_0/\delta\mathbf{R})_{\mathrm{Cu}}$ is small compared to that of oxygen, $S_{\mathrm{O}}=V(\delta e_0/\delta\mathbf{R})_{\mathrm{O}}$. Although the x dependence of the response functions S_{Cu} and S_{O} is different for $x>0.12$ ($e_0>0.1$), both functions are proportional to e_0 for $x<0.12$ (i.e., $S_{\mathrm{Cu}}\propto e_0$ and $S_{\mathrm{O}}\propto e_0$). On the other hand, the energy-level screening response, $S_\lambda=(\delta\lambda_0/\delta\mathbf{R})$, is a direct consequence of charge transfer on the copper sites, usually mediated by an oxygen mode. S_λ varies as powers of e_0^2 for $x<0.12$.

The oxygen breathing mode generates charge transfer between copper atoms. When two oxygen atoms are displaced 180° out of phase with one another, different local environments are created for copper site. These inequivalent copper environments lead to slight accumulation of charge on one site and depletion on the other. As a result, a static copper charge-density wave with wave vector $\mathbf{X}$ is formed, but the amplitude of this wave changes as a function of doping concentration. Because the charge fluctuation is strongly suppressed as half-filling is approached, the amplitude is larger in the metallic regime than near the insulating regime. The electron-phonon transition matrix element for this mode, therefore, depends strongly on concentration. The oxygen breathing mode corresponds to the following parametrization:

$$V_{1,1}=V_{1,2}\neq V_{2,1}=V_{2,2}\ ,$$
$$e_1\neq e_2\ , \tag{A4}$$

and

$$\lambda_1\neq\lambda_2\ .$$

We write the matrix element for the oxygen breathing mode near half-filling ($r_0\to 0$) as

$$g_{\mathrm{X,O}}\approx\tfrac{1}{2}S_\lambda+\frac{8r_0}{\varepsilon_d-\varepsilon_p}(7r_0-S_{\mathrm{O}})\ . \tag{A5}$$

The concentration dependence of the matrix element in Eq. (A5) comes from band renormalizations (r_0 and λ_0) as well as from variational responses (S_{O} and S_λ). Therefore, we can easily deduce, based on counting powers of e_0, that Eq. (A5) varies as e_0^2 near the metal-insulator transition.

In the copper breathing mode, two copper ions are displaced in opposite directions. As a result, this motion leads to a formation of static oxygen CDW. The copper breathing mode corresponds to the parametrization

$$V_{1,1}=V_{2,1}\neq V_{1,2}=V_{2,2}\ ,$$
$$e_1=e_2\ , \tag{A6}$$

and

$$\lambda_1=\lambda_2\ .$$

Because only the oxygen environment is changed, the variational parameters associated with copper sites are identical. Although this copper mode is identical to that of an oxygen mode in many ways, it is translated by a copper-oxygen bond length. This translation leads to the following phase changes in Bloch waves:

$$M_{13}=M^*_{31}=(r_1e^{i\mathbf{k}\cdot\delta\mathbf{R}}-r_0)e^{i\tilde{k}}$$
$$\to(r_2e^{-i\mathbf{k}\cdot\delta\mathbf{R}}-r_0)e^{-i\tilde{k}}\ , \tag{A7a}$$
$$M_{24}=M^*_{42}=(r_2e^{-i\mathbf{k}\cdot\delta\mathbf{R}}-r_0)e^{-i\tilde{k}}$$
$$\to(r_1e^{i\mathbf{k}\cdot\delta\mathbf{R}}-r_0)e^{-i\tilde{k}}\ . \tag{A7b}$$

With these changes, the electron-phonon matrix element near the metal-insulator transition is expressed as

$$g_{\mathrm{X,Cu}}\approx\frac{4r_0^2}{\varepsilon_d-\varepsilon_p}(2\tilde{k}\cos 2\tilde{k}-7\sin 2\tilde{k})\ . \tag{A8}$$

Although the matrix element for copper does not have contributions from the variational responses, its concentration dependence is similar to that of the oxygen breathing mode due to band renormalization effects. [It should be stressed that the absence of the variational response contribution to Eq. (A8) is accidental, due to simplicity of the model.] We shall see later that, when a more realistic model is considered, there are no perfect cancellations. However, as we might expect, the variational response from a static charge-density wave on those sites that are not subject to a strong repulsive potential is generally weak.

Because the copper-oxygen overlap integral is almost unchanged when ions are displaced perpendicularly, the transverse motion of either copper or oxygen ions have smaller matrix elements than for the copper breathing mode. To lowest order, the variation in hybridization depends quadratically on the displacement. In linear response theory, both of these motions lead to almost equivalent electronic responses. This corresponds to

$$V_{1,1}=V_{1,2}=V_{2,1}=V_{2,2}\approx V\ ,$$
$$e_1=e_2\ , \tag{A9}$$

and

$$\lambda_1=\lambda_2\ .$$

The matrix element for these modes near the metal-insulator transition is

$$g_{\mathbf{X},T}\approx\frac{4r_0^4}{(\varepsilon_d-\varepsilon_p)^2}k_z\sin 4\tilde{k}\ . \tag{A10}$$

Here, the z axis is the direction perpendicular to the chain. As might be expected, there are no contributions from the variational responses, here. The concentration dependence of the transition matrix element, therefore, is entirely from renormalized band structure. Furthermore, we can easily see that the x dependence of the matrix element is negligible because of the lack of a distortion-induced electronic response.

APPENDIX B: 2D ELECTRON-PHONON TRANSITION MATRIX ELEMENTS

As in one dimension, we consider the scattering processes between states $\alpha_{k,\sigma}$ and $\alpha_{k+Q,\sigma}$, and express these quasiparticle states explicitly in terms of a linear combination of $3d_{x^2-y^2}$, $2p_x$, and $2p_y$ orbitals

$$\alpha_{k,\sigma}=A^+(D_{1,k,\sigma}+D_{2,k,\sigma})+B_x^+C_{x_1,k,\sigma}+B_x^{+*}C_{x_2,k,\sigma}+B_y^+C_{y_1,k,\sigma}+B_y^{+*}C_{y_2,k,\sigma} \tag{B1a}$$

and

$$\alpha_{k+Q,\sigma}=A^-(D_{1,k,\sigma}-D_{2,k,\sigma})+B_x^-C_{x_1,k,\sigma}+B_x^{-*}C_{x_2,k,\sigma}+B_x^-C_{x_1,k,\sigma}+B_x^{-*}C_{x_2,k,\sigma}\ . \tag{B1b}$$

Here, the coherence factors $A^\pm$ and $B_\eta^\pm$ measure the copper and oxygen contribution to a quasiparticle state. An asterisk ($*$) denotes the complex conjugate, and the superscripts ($+$ and $-$) are used to indicate the elements of the first and second row in the unitary matrix.

In order to derive Eqs. (2.11), we determine the overlap integrals V and t as a function of the separation distance and orientation by using the results of Slater and Koster.[28] Because d and p orbitals are highly directional, the overlap integrals depend strongly on the relative orientation of these orbitals. This is nicely illustrated in the orientation dependence of oxygen-oxygen overlap integral

$$t(p_x,p_y)=\bar{l}\,\bar{m}V_{pp\sigma}-\bar{l}\,\bar{m}V_{pp\pi} \tag{B2a}$$

and the copper-oxygen hybridization

$$V(p_x,d_{x^2-y^2})=\frac{\sqrt{3}}{2}\bar{l}(\bar{l}^2-\bar{m}^2)V_{pd\sigma}+\bar{l}(\bar{l}-\bar{l}^2+\bar{m}^2)V_{pd\pi}\ , \tag{B2b}$$

$$V(p_y,d_{x^2-y^2})=\frac{\sqrt{3}}{2}\bar{m}(\bar{l}^2-\bar{m}^2)V_{pd\sigma}+\bar{m}(\bar{l}+\bar{l}^2-\bar{m}^2)V_{pd\pi}\ . \tag{B2c}$$

Here, the relative orientation of two overlapping orbitals are denoted by $\bar{l}$, $\bar{m}$, and $\bar{n}$ where $\mathbf{d}=\bar{l}\,\hat{\mathbf{x}}+\bar{m}\,\hat{\mathbf{y}}+\bar{n}\,\hat{\mathbf{z}}$. As we might expect, the overlap integral between orbitals $d_{x^2-y^2}$ and $p_{x,y}$, and between p_x and p_y also depends strongly on the separation distance

$$V_{pd\sigma(\pi)}=\zeta_{pd\sigma(\pi)}\frac{1}{m}\frac{r_d^{3/2}}{d^{7/2}}\ ,$$
$$V_{pp\sigma(\pi)}=\zeta_{pp\sigma(\pi)}\frac{1}{m}\frac{1}{d^2}\ , \tag{B2d}$$

where ζ is a constant which is determined by the types of bonds between the two orbitals. Although the hybridization integrals (V and t) have both π and σ bond contributions, these details are not necessary for the purpose of our calculation. When the distortion is small, we can reexpress the changes (in hybridization) in terms of the undistorted values V and t. We calculate the changes in the copper-oxygen as well as the oxygen-oxygen overlap to lowest order in displacement by expanding Eqs. (B2).

Expressing the antibonding state in terms of coherence factors $A^\pm$ and $B^\pm$, which depend on dopant concentration, we examine the x dependence of the matrix element for each $\mathbf{X}$ phonon shown in Fig. 2 by evaluating Eq. (2.10b). When the antibonding band is half full, the states near E_F are copperlike with no oxygen mixture (i.e., $A^\pm=1$ and $B^\pm=0$). When holes are added to this band, however, the copperlike states near E_F become somewhat oxygenlike. This implies $B_\eta^\pm$ increases while $A^\pm$ decreases by the same amount. Since $A^\pm$ and $B^\pm$ are elements of a unitary matrix, we can easily calculate their dependence on the Bose amplitude e_0. To lowest order in e_0, $B^\pm$ varies linearly with e_0 while $A^\pm$ is almost a constant. Therefore, we can easily see the concentration dependence of the matrix elements by counting the number of $B_\eta^\pm$'s.

A planar copper mode is shown in Fig. 2(a). The frequencies of these modes, calculated by the LDA approach, range from 6 to 60 meV and the phonon density is a maximum at roughly 20 meV. However, the actual measured value differs somewhat from this because screening effects are not fully accounted for in LDA calculations. The copper mode shown in Fig. 2(a) is equivalent to that of a one-dimensional breathing mode which creates a different local environment for oxygen sites (for $2p_x$ and $2p_y$ orbital sites) while maintaining identical copper sites. Therefore, this mode generates a static oxygen CDW by transferring charge from one oxygen site to another. We write the matrix element for this mode as

$$g_{\mathbf{X},M_1}=4\sum_\eta\left[\sqrt{2}S_{\mathrm{Cu}}I_{a,\eta}^+ + ir_0\left[k_x'I_{b,\eta}^- - \frac{7}{\sqrt{2}V}I_{c,\eta}^+\right]\right]\ . \tag{B3}$$

We express the various orbital contributions to the ma-

trix element in terms of coherence factors $A^{\pm}$ and $B^{\pm}$

$$I^{\pm}_{a,\eta} = A^{-}B^{+'}_{\eta}\cos\tilde{k}_{\eta} \pm A^{+}B^{-''}_{\eta}\sin\tilde{k}_{\eta} , \tag{B4a}$$

$$I^{\pm}_{b,\eta} = A^{-}B^{+''}_{\eta}\sin\tilde{k}_{\eta} \pm A^{+}B^{-'}_{\eta}\cos\tilde{k}_{\eta} , \tag{B4b}$$

$$I^{\pm}_{c,\eta} = A^{-}B^{+''}_{\eta}\cos\tilde{k}_{\eta} \pm A^{+}B^{-'}_{\eta}\sin\tilde{k}_{\eta} , \tag{B4c}$$

$$I^{\pm}_{d,\eta} = A^{-}B^{+'}_{\eta}\sin\tilde{k}_{\eta} \pm A^{+}B^{-''}_{\eta}\cos\tilde{k}_{\eta} . \tag{B4d}$$

Although the $A^{\pm}$'s are real, the $B^{\pm}_{\eta}$'s are complex. Hence, we separate $B^{\pm}$ in terms of real and imaginary components $B^{\pm}_{\eta} = B^{\pm'}_{\eta} + iB^{\pm''}_{\eta}$. We use the notation

$$\tilde{k}_x = \frac{1}{\sqrt{2}}(\tilde{k}'_x - \tilde{k}'_y), \quad \tilde{k}_y = \frac{1}{\sqrt{2}}(\tilde{k}'_x + \tilde{k}'_y) \tag{B5}$$

to simplify the expression. A single prime on k_{η} denotes the momentum in the reduced BZ corresponding to a distorted lattice having a frozen **X** phonon. By counting the powers of e_0, we see that the x dependence of this matrix element varies as e_0^2 as half-filling is approached.

In Fig. 2(b), we show the oxygen quadrupolar mode. Although this mode appears to transfer charge between copper sites, all copper sites remain identical. Furthermore, all oxygen sites remain equivalent, as well. The frequency for this mode is 100 meV, and the density of states is low. The matrix element for this mode is given by

$$g_{\mathbf{X},M_2} = 4\left[\sum_{\eta}(S_{\mathrm{O}}I^{+}_{a,\eta} - 7r_0 I^{+}_{b,\eta}) - r_0(\tilde{k}_x I^{-}_{c,x} - \tilde{k}_y I^{-}_{c,y}) + \sqrt{2}t(\Xi^{-}\tilde{k}'_x\cos\tilde{k}'_y - \Xi^{+}\tilde{k}'_y\cos\tilde{k}'_x)\right] , \tag{B6}$$

where $\Xi^{\pm} = \Delta_{x,y} \pm \Delta_{y,x}$ and $\Delta_{\alpha,\beta} = B^{+'}_{\alpha}B^{-''}_{\beta} + B^{-'}_{\alpha}B^{+''}_{\beta}$. Because the oxygen motion leads to the variational response S_{O}, the concentration dependence (based on power counting arguments for e_0) of the matrix element is similar to that of the M_1 mode, but the amplitude is expected to be smaller since there is no CDW on either copper or oxygen sites.

The copper and oxygen transverse modes are shown in Figs. 2(c) and 2(d), respectively. When either of these ions is displaced in the perpendicular direction to the plane, all sites (both copper and oxygen) remain equivalent because these distortions do not change the overlap integrals. The electronic responses, therefore, are similar for both of these modes. The normal mode frequencies for the copper motion range from 20 to 80 meV. The transition matrix element for this mode is written as

$$g_{\mathbf{X},M_3} = i4r_0 k'_z \sum_{\eta} I^{-}_{a,\eta} . \tag{B7}$$

The oxygen, on the other hand, has a frequency range (10–75 meV) similar to copper, and the matrix element is given by

$$g_{\mathbf{X},M_4} = -4k'_z\left[r_0\sum_{\eta} I^{-}_{d,\eta} + 2t\Xi^{+}\cos\tilde{k}'_x\right] . \tag{B8}$$

The vertical component of a wave vector k'_z in Eqs. (B7) and (B8) is obtained by assuming periodicity of the copper-oxide layers in the z direction. We set k'_z to a constant of order unity in our later calculations. As we might have expected, there are no contributions from the variational responses (S_{Cu}, S_{O}, and S_{λ}) in Eqs. (B7) and (B8). As a result, these modes couple weakly (if they couple at all) to electrons by way of Bloch wave shifts. The power counting argument, again, shows that these modes behave as e_0^2.

In Figs. 2(e) and 2(f), we show two oxygen modes which transfer charge between copper sites. Similar to our earlier discussion on the oxygen breathing mode in one dimension, the charge-transfer effect in these modes generates a stronger response than the other four modes we have discussed above. Because of Coulomb correlations on copper sites, the formation of a static copper CDW is energetically unfavorable. When charges are transferred onto a copper site, the energy level must be renormalized to avoid the infinite Coulomb repulsion. As a result, the energy-level renormalization becomes the dominant source of scattering. There are 2 such modes (out of 21) with frequencies 74 and 88 meV. The matrix element is given by

$$g_{\mathbf{X},M_5} = S_{\lambda}A^{+}A^{-} + 4\sum_{\eta}(7r_0 - S_{\mathrm{O}})\xi_x I^{+}_{b,\eta} + 4r_0(k_1 I^{-}_{d,x} + k_2 I^{-}_{d,y}) + 4t\left[4\Theta^{-}\sin\tilde{k}'_y\sum_{\eta}\xi_{\eta} + (k_1\Lambda^{-+} + k_2\Lambda^{+-})\prod_{\eta}\sin\tilde{k}_{\eta} - (k_2\Lambda^{-+} + k_1\Lambda^{+-})\prod_{\eta}\cos\tilde{k}_{\eta}\right] , \tag{B9}$$

where $k_1 = k_x\xi_x - k_y\xi_y$, $k_2 = k_y\xi_x - k_x\xi_y$. Here ξ_{η} denotes the normalized components of the oxygen displacement. We define $\Theta^{\pm} = \Lambda^{-+} \pm \Lambda^{+-}$, and $\Lambda^{\alpha\beta} = B^{\alpha'}_{x}B^{\beta''}_{y} + B^{\alpha'}_{y}B^{\beta''}_{x}$. The two-dimensional oxygen breathing mode shown in Fig. 2(f) has[26] the frequency 140 meV (this is large compared to the measured value of 90 meV). This mode leads to a similar renormalization response to that of the M_5 mode. We write the matrix element as

$$g_{\mathbf{X},M_6} = S_{\lambda}A^{+}A^{-} + 4\sum_{\eta}[(7r_0 - S_{\mathrm{O}})I^{+}_{a,\eta} + r_0 k_{\eta} I^{-}_{d,\eta}] + 8t\sum_{\eta}[\Delta_{x,y}\cos\tilde{k}_y(2\sin\tilde{k}_x - \tilde{k}_{\eta}\cos\tilde{k}_x) + \Delta_{y,x}\sin\tilde{k}_y(2\cos\tilde{k}_x + \tilde{k}_{\eta}\sin\tilde{k}_x)] . \tag{B10}$$

These transition matrix elements in Eqs. (B9) and (B10) appear rather complicated because, when oxygen ions in two dimensions are displaced, the copper-oxygen hybridizations as well as the oxygen-oxygen hopping integrals are usually changed together. Because the oxygen motion in these modes is similar, both matrix elements in Eqs. (B9) and (B10) involve the variational responses S_{λ} and S_{O}, which reflect the screening effect of the renormalization of the bare copper level and hybridization integral.

*Present address: Department of Physics and Astronomy, The Johns Hopkins University, Baltimore, MD 21218.

†Present address: Physics Department 510A, Brookhaven National Laboratory, Upton, NY 11973, and Physics Department, SUNY, Stony Brook, NY 11794.

[1]P. W. Anderson, Science **235**, 1196 (1987); R. B. Laughlin, Phys. Rev. Lett. **60**, 2677 (1988); R. Zeyher and G. Zwicknagle, Solid State Commun. **66**, 617 (1988).

[2]C. G. Olson, R. Liu, A. B. Yang, D. W. Lynch, A. J. Arko, R. S. List, B. W. Veal, Y. C. Change, P. Z. Jiang, and A. P. Paulikas, Science **245**, 731 (1989); R. Manzke, T. Buslaps, R. Claessen, and J. Fink, Europhys. Lett. **9**, 477 (1989).

[3]J. P. Lu, Q. Si, J. H. Kim, and K. Levin, Phys. Rev. Lett. **65**, 2466 (1990).

[4]J. H. Kim, K. Levin, R. Wentzcovitch, and A. Auerbach, Phys. Rev. B **40**, 11 378 (1989).

[5]Q. Si, J. H. Kim, J. P. Lu, and K. Levin, Phys. Rev. B **42**, 1033 (1990).

[6]A. T. Fiory, S. Martin, R. M. Fleming, L. F. Schneemeyer, J. V. Wasczak, A. F. Hebard, and S. A. Sunshine, Physica C **162-164**, 1195 (1989).

[7]T. Imai, T. Shimizu, H. Yasuoka, Y. Ueda, K. Yoshimura, and K. Kosuga, Physica C **162-164**, 169 (1989).

[8]C. C. Tsuei, Proceedings of the 3rd Bar Ilan Conference on Frontiers in Condensed Matter Physics, Israel, 1990 (unpublished); Physica A (to be published).

[9]K. Levin, Ju H. Kim, J. P. Lu, Q. Si, Physica C **175**, 449 (1991); J. H. Kim, K. Levin, and A. Auerbach, Phys. Rev. B **39**, 11 633 (1989).

[10]A. T. Fiory, and G. S. Grader, Phys. Rev. B **38**, 9198 (1988); A. Fert and P. M. Levy, *ibid.* **36**, 1907 (1987).

[11]P. W. Anderson and Z. Zou, Phys. Rev. Lett. **60**, 132 (1988); P. A. Lee and N. Read, *ibid.* **58**, 2691 (1987); P. A. Lee, *ibid.* **63**, 680 (1989); N. Nagaosa and P. A. Lee, *ibid.* **64**, 2450 (1990); L. B. Ioffe and P. B. Wiegmann, Phys. Rev. Lett. **65**, 653 (1990).

[12]M. Gurvitch and A. T. Fiory, Phys. Rev. Lett. **59**, 1337 (1987), and references therein.

[13]M. Suzuki, in *Strong Correlation and Superconductivity,* edited by H. Fukuyama, S. Maekawa, and A. P. Malozemoff, (Springer-Verlag, New York, 1989).

[14]K. Kamaras, S. L. Herr, C. D. Porter, N. Tache, D. P. Tanner, S. Etemad, T. Venkatesan, E. Chase, A. Inam, X. D. Wu, M. S. Hedge, and B. Dutta, Phys. Rev. Lett. **64**, 84 (1990).

[15]See, for example, D. Pines, *Elementary Excitations in Solids* (Benjamin-Cummings, Reading, 1963); N. W. Ashcroft and N. D. Mermin, *Solid State Physics* (Saunders College, Philadelphia, 1976).

[16]J. Orenstein, G. A. Thomas, A. J. Millis, S. L. Cooper, D. H. Rapkine, T. Timusk, L. F. Schneemeyer, and J. V. Wasczak, Phys. Rev. B **42**, 6342 (1990).

[17]B. Ellman, H. M. Jaeger, D. P. Katz, T. F. Rosenbaum, A. S. Copper, and G. P. Espinosa, Phys. Rev. B **39**, 9012 (1989).

[18]P. B. Allen, W. E. Pickett, and H. Krakauer, Phys. Rev. B **36**, 3926 (1987); **37**, 7482 (1988); P. B. Allen, *ibid.* **17**, 3725 (1979).

[19]N. F. Mott and E. A. Davis, *Electronic Processes in Non-Crystalline Materials* (Clarendon, Oxford, 1979); A. F. Ioffe and A. R. Regel, Prog. Semicond. **4**, 237 (1960).

[20]Some suggestions of the importance of correlation effects in electron-phonon interactions were made by Cohen and coworkers who found that they affected the instability of the oxygen breathing mode [see, for example, R. E. Cohen, W. E. Pickett, and H. Krakauer, Phys. Rev. Lett. **62**, 831 (1989)].

[21]C. L. Fu and A. J. Freeman, Phys. Rev. B **35**, 8861 (1987); A. Muramatsu, and W. Hanke, *ibid.* **38**, 878 (1988); J. Ashkenazi, D. Dacorogna, and M. Peter, Solid State Commun. **29**, 181 (1979).

[22]A. K. McMahan, R. M. Martin, and S. Satpathy, Phys. Rev. B **38**, 6650 (1988).

[23]D. M. Newns, M. Rasolt, and P. Pattnaik, Phys. Rev. B **38**, 6513 (1988).

[24]R. E. Watson, H. Ehrenreich, and L. Hodges, Phys. Rev. Lett. **24**, 829 (1970); J. C. Slater, and G. F. Koster, Phys. Rev. **94**, 1498 (1954).

[25]P. Coleman, Phys. Rev. B **29**, 3035 (1984); S. E. Barnes, J. Phys. F **6**, 1375 (1976); **7**, 2632 (1977).

[26]R. E. Cohen, W. E. Pickett, H. Krakauer, and L. L. Boyer, Physica B **150**, 61 (1988).

[27]The rotational and tilting modes are among these unstable modes. It should be noted that the tilting mode is thought to be responsible for the tetragonal-orthorhombic transition. Although careful modeling of these unstable modes with strong Coulomb correlations would be interesting, we will not consider them here.

[28]First, we change the amplitude of the static displacement of either the copper or oxygen ions and then calculate e_n and λ_n from the mean-field equations for $H_{\rm FP}^{2d}$ at each E_F. Finally, we extract $\delta e_0/\delta R$ and $\delta\lambda_0/\delta R$ by comparing e_n and λ_n to e_0 and λ_0 as a function of the displacement. As we might expect, each phonon mode leads to a different response. We, therefore, consider each **X** mode separately.

[29]For simplicity, in evaluating $\langle\langle g_{\mathbf{X},M_i} \rangle\rangle_{\rm FS}$ in two dimensions, we use one-dimensional results for the value of the variational response functions (see J. H. Kim, Ph.D. thesis, University of Chicago, 1990). Because the Coulomb correlations are included in the one-dimensional model, this approximation may lead to only minor changes in $\langle\langle g_{\mathbf{X},M_i} \rangle\rangle_{\rm FS}$.

[30]J. Keller, R. Bulla, Th. Hohn, and K. W. Becker, Phys. Rev. B **41**, 1878 (1990).

[31]G. Kotliar, P. A. Lee, and N. Read, Physica C **153-155**, 538 (1988).

[32]M. B. Maple (private communication); Y. Iye (unpublished); Physica B **163**, 63 (1990).

[33]B. Ranker, F. Gompf, E. Gering, N. Nucker, D. Ewert, W. Reichardt, and H. Rietschel, Z. Phys. B **15**, (1987).

[34]J. L. Martins and M. L. Cohen, Phys. Rev. B **37**, 3304 (1988).

[35]S. Tajima, S. Uchida, H. Ishii, H. Takagi, S. Tanaka, U. Kawabe, H. Hasagawa, T. Aita, and T. Ishiba, Mod. Phys. Lett. B **1**, 353 (1988).

[36]Z. Schlesinger, R. T. Collins, D. L. Kaiser, and F. Holtzberg, Phys. Rev. Lett. **59**, 1958 (1987).

[37]J. M. Tarascon, L. H. Greene, W. R. McKinnon, G. W. Hull, and T. H. Geballe, Science **235**, 1373 (1987).

[38]M. Suzuki, Phys. Rev. B **39**, 2312 (1989).

[39]C. Uher, A. B. Kaiser, E. Gmelin, and L. Walz, Phys. Rev. B **36**, 5676 (1987).

[40]J. M. Ziman, *Electrons and Phonons* (Clarendon, Oxford, 1967).

[41]See, for example, A. B. Kaiser and S. Doniach, Int. J. Magn. **1**, 11 (1970).